UNIVERSITÀ
DEGLI STUDI
FIRENZE

Università degli Studi di Firenze
Dipartimento di Ingegneria dell'Informazione (DINFO)
Corso di Dottorato in Ingegneria dell'Informazione
Curriculum: Telecomunicazioni e Sistemi Telematici

Vehicular and Positioning Visible Light Systems with Low-cost LED-based Devices

Candidate
Patrizio Marcocci

Supervisor
Prof. Lorenzo Mucchi

PhD Coordinator
Prof. Luigi Chisci

ciclo XXXI, 2016-2018

Università degli Studi di Firenze, Dipartimento di Ingegneria
dell'Informazione (DINFO).

Alla mia cara e amata nonna Irma.

Acknowledgments

I would like to thank my supervisor Dr. Lorenzo Mucchi and Dr. Luca Simone Ronga for their guidance and expertise. A great thank you to all my colleagues at the Signal Processing and Communications Laboratory (LESC) and CNIT research unit of the University of Florence. A special mention goes to Dr. Dasara Shullani, Eng. Gabriele Fabbri and Dr. Sara Jayousi for their friendly support and essential encouragement. I owe my deepest gratitude to my friend and colleague Dr. Alessio Martinelli for his daily fraternal advices and motivation all over years, without which I wouldn't have been able to challenge myself like I've done.

I would also like to thank Dr. Domenico Giustiniano for his helpful guidance and advices during my visiting period at IMDEA Networks Institute of Leganés, Madrid. I am immensely grateful to my colleagues and friends Eng. Ander Galisteo Zabalo and Eng. Diego Juara Casero for their essential collaboration, precious help and closeness during my internship at IMDEA: ¿qué habría hecho sin vosotros, tíos?

I am deeply grateful to my sweet friends Bárbara Gonzáles Barrionuevo and Irene Cortés Lafuente for their lovely support, affection, empathy and for making me feel at home during the extremely pleasant year we spent living together in Leganés: ¡os echo de menos chichas!

I am grateful as well to my closest friends Davide Biagiotti, Francesco Gentiloni and Salvatore Leccese for their encouragement, advices, closeness and support, in every-single-day.

Finally, to my adorable parents Mauro and Daniela for their incommensurable love and teaching: vi voglio un mondo di bene!

Abstract

Artificial lighting is everywhere, from the light bulbs on our ceilings to car headlights. This makes Visible Light Communication (VLC) an attracting technology since it uses modulated optical radiation in the visible light spectrum, exploiting the light emission of LEDs. The main advantage of VLC is that it can provide both standard illumination and data connection. Also VLC systems are suitable for many different applications due to their relatively simple design for basic functioning, efficiency and large geographical distribution. Recently both Vehicular VLC (V^2LC) and LED-based Positioning Systems (LPS) are gaining a lot of attention from industry and the scientific community due to their great potential in terms of driver safety and positioning accuracy, respectively.

The aim of this PhD dissertation is to investigate two different VLC systems: a V^2LC system and an LPS technique. Both are designed for using low-cost components and for being analyzed in realistic environments by exploiting two dedicated testbeds. An LED-based traffic light for sending traffic and safety information, and a 2D localization algorithm implemented on an open source platform (OpenVLC), are studied.

For the V^2LC topic, after a preliminary study of a simple propagation VLC channel, an IEEE 802.15.7-complaint low-cost software-defined transceiver along with an experimental VLC application are presented. The transceiver implements the specific standard PHY-level for outdoor VLC and it is able to stream data at 100 kbit/s.

For the positioning system, a new multipath detection technique for filtering out reflections and better positioning with light is designed and tested in realistic scenarios. More in details, the multipath detection does not require the knowledge of the channel impulse response, and that it is suited to be implemented in low-cost positioning receivers that use a single photodiode. To develop this technique, (i) the statistical properties of Non-Line-of-Sight (NLOS) components is analyzed, (ii) an automated testbed to study the reflections of different types of surfaces and materials is developed, and (iii) an algorithm to remove the NLOS components affecting the positioning is designed. Experimental evaluation shows that in complex environments this methodology can reduce the localization error using a single photodiode up to 93%.

Contents

Chapter 1

Introduction

1.1 Motivations

Artificial lighting is everywhere, from the light bulbs on our ceilings to car headlights. Visible Light Communication (VLC) is a promising and attractive technology as it uses modulated optical radiation in the visible light spectrum. VLC exploits the light emission of fast-switching sources like LEDs (Light Emission Diodes), providing both standard illumination and data connection, at the same time. As rule of thumb, each LED that is being used for lighting can be used also for transmitting data.

Generally speaking VLC technology is still in its infancy as is being researched since 2003 [31]. Recently both the research community and the industrial companies have started to invest their time and money after LEDs became much more affordable and widely used (last 5 years) in almost all the lighting applications. VLC has a great potential for many applications due to their relatively simple design for basic functioning, efficiency and large geographical distribution. Since the human eye perceives only the average intensity when light is switched on and off fast enough, then it is possible to transmit information data using LEDs without a notable effect on the light illumination level by humans. Recent advances in materials and solid-state technologies have enabled the development of highly efficient LEDs that are now being widely used both in indoor and outdoor lighting and signaling. Lately both Vehicular VLC (V^2LC) and LED-based Positioning Systems (LPS) are gaining a lot of attention from industry and the scientific community due to their great potential in terms of driver safety and positioning

accuracy, respectively.

The automotive industry is under a major change and new vehicles are being enriched by the recent advances in communication. Transportation is becoming more intelligent with smart roads that connect smart cars (see Fig. 1.1). Moreover, in the context of an increasing interest towards reducing the number of traffic accidents and of associated victims, communication-based vehicle safety applications have merged as one of the best solutions to enhance road safety. Actual vehicular system, like Intelligent Transportation System (ITS) and Intelligent Traffic System (ITF), are based on radio frequency (RF) and typically suffer from the lack of spectrum. Furthermore, many automotive manufacturers have started to employ LEDs due to their high resistance to vibration, improved safety performance, and long life span. LEDs can be now found in brake lights, turn signals, and headlamps in most of new vehicles. The outdoor and on-vehicle omnipresence of LEDs makes the use of VLC for vehicular communications feasible.

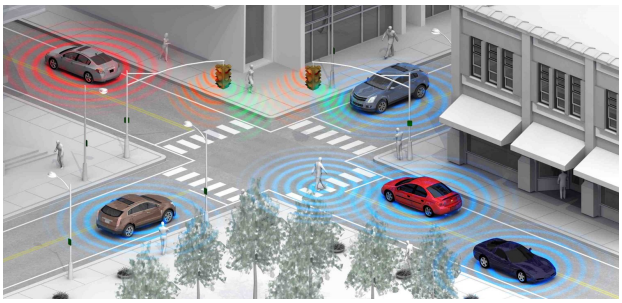

Figure 1.1: Vehicular intelligent system.

The widespread usage of LEDs for illumination constitutes an opportunity to design ubiquitous and economical positioning systems. LPS might be a solution for positioning with better accuracy with respect to traditional RF-based systems given the great capillarity of VLC transmitters (see Fig. 1.2). LPS can easily be integrated into the existing lighting infrastructure (i.e., facilitates the reuse of existing infrastructure) for the purpose of localization in addition to its essential function of illumination, typically without requiring rewiring. It is also important to note that positioning systems can be deployed not only for indoor applications, but also for outdoor applications such as street lights, car lights, and airport taxi-way lighting [47]. However, one of the reasons for finding new positioning techniques using vis-

ible light is not just about the current limitations of RF-based techniques, but also the prospects of exploiting VLC in the Internet of Things (IoT) paradigm. For these reasons VLC requires continuous effort to overcome

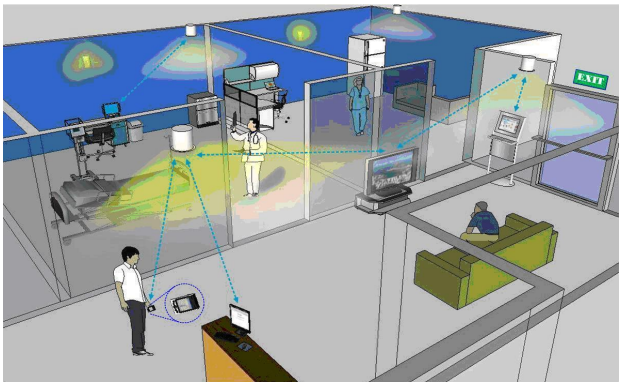

Figure 1.2: LED-based Positioning System scenario.

challenges, especially in automotive communications and positioning applications. Finally, it is important to note that the state-of-the-art lacks of a proper study of such VLC systems in realistic conditions, since to date the majority of research has aimed at achieving and demonstrating high data rates capable to outclass existent RF communication systems [20].

1.2 Objectives

This PhD dissertation has two main objectives as it involves two different VLC systems: a V^2LC system and an LPS technique. For both automotive and positioning applications proper experimental campaigns will help investigating issues in realistic environments. The first goal is to exploit a COTS (Commercial Off The Shelf) LED-based traffic light as a VLC transmitter for analysing the vehicular channel in a realistic scenario and, at the same time, sending traffic and safety information to vehicles. The second goal is the analysis of a 2D (two-dimensional) relative positioning algorithm in the presence of multipath (i.e. object reflections). As the first goal, also this one is based on a measurement campaign in realistic scenarios.

1.3 Contributions

The main contributions of this thesis are the following:

- Chapter. 5: a preliminary study of a simple propagation VLC channel and the design and the implementation of a VLC transceiver for vehicular applications. In particular, a propagation channel model of a simple visible light system through an experimental measurement campaign is presented; and an IEEE 802.15.7 PHY-I compliant physical layer is developed with a Software Defined Radio (SDR) toolkit (i.e. GNURadio).

- Chapter. 6: investigation of the multipath effect on a 2D relative positioning VLC system. Different type of materials are employed in realistic mobile scenarios for understanding the impact of reflections and studying and proposing countermeasures against the positioning error due to multipath. This part proposes a new multipath detection technique for positioning with light that does not require the knowledge of the channel impulse response, and that it is suited to be implemented in low-cost positioning receivers that use a single photodiode.

The second subject refers to an 11-month internship at the IMDEA Networks Institute (Leganés, Madrid, Spain). More in details, the following arguments are investigated:

1. VLC vehicular and positioning system state of the art revision:
    - Non-Line-Of-Sight (NLOS) propagation analysis in vehicular VLC systems;
    - impact of reflection in a VLC positioning system;
    - usage and analysis of light polarizer in VLC systems.
2. OpenVLC platform[1] receiver ADC (Analog-to-Digital Converter) stage analysis:
    - acquisition and sampling process analysis;
    - electrical circuit design and revision;
    - data storage design and implementation.

[1] For details, please refer to Sec. 4.3.1.

3. Experimental study:
    - testbed setup and validation test performing;
    - test campaign performing.
4. Acquired data set processing:
    - characterization and detection of material reflections (i.e. NLOS path detection);
    - multipath effect analysis on a two-dimension (2D) relative positioning algorithm with a single low-cost LED;
    - design and development of an algorithm for filtering out reflections.

Chapter 2

Visible Light Communications, the Internet of Light

This chapter gives an overview of the technology called Visible Light Communication (also know as VLC or "Li-Fi", Light Fidelity), a relatively new wireless optical communication technique that exploits the visible light emitted by LEDs. Along the chapter a brief introduction of the IEEE standard for VLC is given as well as a discussion of the advantages and challenges of this breakthrough technology compared to classic radio-frequency solutions.

2.1 Background

The solid-state lighting is a game changer for indoor illumination. Current incandescent and fluorescent lamps are being replaced by LEDs at a rapid pace (see Fig. 2.1). Apart from extremely high energy efficiency, LEDs have other advantages such as longer lifespan, lower heat generation and improved color rendering without using harmful chemicals. One additional benefit of LEDs is that they are capable of switching to different light intensity at a very fast rate, as fast as the human eye can notice any variation. This functionality has given rise to a novel communication technology (known as Visible Light Communication, VLC or "Li-Fi"[1]) where LED luminaries can

[1]Professor Harald Haas, Chair Professor of Mobile Communications at the University of Edinburgh and co-founder of "pureLiFi", coined the term "Li-Fi" (Light Fidelity) at his

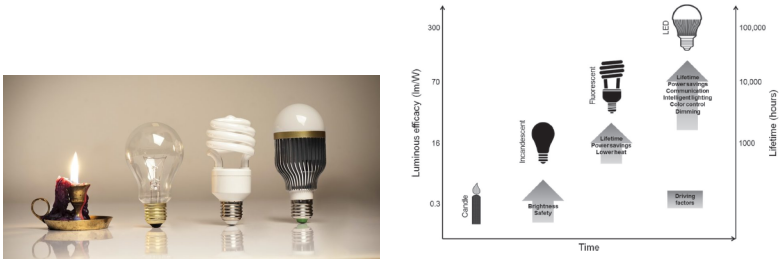

(a) (b)

Figure 2.1: Development of illumination technology. Artificial illumination evolution (left), efficacy and lifetime evolution [73] (right).

be used for high speed data transfer.

VLC is an emerging field in Optical Wireless Communication (OWC) which utilizes the superior modulation bandwidth of LEDs to transmit data. In modern day communication systems, the most popular frequency band is Radio Frequency (RF) mainly due to little interference and good coverage. However, the rapidly dwindling RF spectrum along with increasing wireless network traffic has leaded to the need of greater bandwidth and spectral relief. By combining illumination and communication, VLC provides ubiquitous communication while addressing the short-falls and limitations of RF communication [46]. VLC technology is anyway fully compatible with RF communications and the two can complement each other, forming hybrid or heterogeneous networks and further enhancing the communication performances. In the last few years, VLC research has shown that it is capable of achieving very high data rates (nearly 100 Mbps in IEEE 802.15.7 standard and up to multiple Gbps in research), indoor localization, device-to-device (D2D) communication with LCD screens or camera sensors, traffic control between traffic lights and vehicles or traffic signals among vehicles, special applications in electromagnetic-sensitive environments such as hospitals, airplanes, and the underground mining industry [46]. For these capabilities and its versatility, VLC has become another potential candidate technology for fifth generation (5G) networks. For instance, in outdoor environment VLC can provide internet hot spots using street lighting and mobile access as part

2011 TED Global Talk where he introduced the idea of “wireless data from every light”.

of the 5G technology in highly congested areas, and within indoor environment it can be used for localization and small cells coverage networks.

2.1.1 Comparison between VLC and RF systems

Even with efficient frequency and spatial reuse, the current RF spectrum is expected to be scarce to meet the near future increasing user traffic demand. Compared to this, the visible light spectrum which includes hundreds of terahertz of license free bandwidth (see Fig. 2.2) is completely untapped for communication. VLC can complement the RF-based mobile commu-

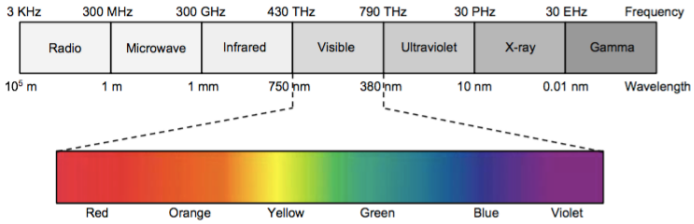

Figure 2.2: Visible light spectrum [73].

nication systems in designing high-capacity mobile data networks. Due to its high frequency, visible light cannot penetrate through most objects and walls creating small cells (or areas) of LED transmitters with no intercell interference issues beyond the walls. Moreover, the inability of visible light to penetrate through the walls provides an inherent wireless communication security. Finally, VLC facilitates the reuse of existing lighting infrastructure for the purpose of communication. This means that such systems can be deployed with relatively lesser effort and at a lower cost [73].
Hence, the most important advantages of VLC technology can be listed as below:

- spectrum crunch alleviation;
- interference absence;
- security enhance;
- spatial reuse possible;
- safety of VLC transmission for human beings;

- energy efficiency of LEDs;
- easy implementation into existing infrastructure;
- low cost devices.

Fifth generation wireless systems represent the novelty in next mobile telecommunications, beyond the current diffuse 4G standard. Compared to the existing 4G systems, 5G systems should achieve much higher capacity, data rate, spectral efficiency, energy efficiency, and user real-time experience. Concurrently, lower battery consumption and lower implementation costs are also deemed to be a must. Small cell has emerged as one of the most promising 5G technologies due to its ability to significantly increase the network capacity/coverage, extend the battery life of mobile devices, and achieve high network energy efficiency. Millimeter-wave (mmWave) spectrum, with a small coverage area and abundant available bandwidth, has been one the firsts technologies to become a promising candidate for 5G networks to enable gigabit-per-second data transmission with the frequency range from 3 to 300 GHz [34]. Although the mmWave spectrum is aimed at high-speed short-range communications in both indoor and outdoor areas, wireless networks will eventually face a capacity explosion that could even overstretch the mmWave spectrum. This motivates the research community to continue exploring new technologies and new architectures for 5G systems as VLC. Moreover, mmWave has no evident propagation advantages over VLC, especially in the indoor scenario, since the very strong penetration loss of both technologies. Generally speaking, VLC can take advantage of free licenses, low cost implementation and low power consumption [34]. A general "RF vs VLC" comparison summary is reported in Table 2.1. These reasons, primarily the spectral and bandwidth drawbacks of RF communication, motivates the use of visible band for communication purposes.

2.1.2 Typical VLC links and types of reflection

The simplest typical VLC system features a point-to-point scheme: a transmitter (TX, i.e. an LED) emits visible light towards a receiver (RX, i.e. a photodiode) which detects the signal. This wireless connection link can be classified into two categories:

- Line-Of-Sight (LOS) link: where a transmitter is within the receiver Field Of View (FOV);

Table 2.1: Comparison of VLC to RF [46] and [80].

Characteristic	**RF**	**VLC**
Available spectrum	$\sim$ 300 GHz	$\sim$ 400 THz
License	Licensed	Unlicensed
Safety	Intensity regulated	Unregulated
Noise interference	Little	High
Security	Limited	High
Coverage	Wide	Limited
Multipath	High	Low
System complexity	High	Low
Electromagnetic interference	Yes	No
Ambient light	Not affected	Sensitive
Weather conditions	Robust	Sensitive
Infrastructure	Access point	Illumination
Power consumption	Medium	Low

- Non-Line-Of-Sight (NLOS) link: relying generally upon the reflection of the light from the ceiling or some other diffusely reflecting surfaces.

The path loss of the NLOS link is generally much larger, while link robustness and ease of use increase, allowing the link to operate even when barriers, such as people or other posts, stand between the transmitter and receiver. When light hits a surface, there are three possible outcomes. Light may be absorbed by the material, it may be transmitted through the surface or it may be reflected. Materials often show some mix of these behaviors, with the proportion of light that goes to each component depending on the properties of the material, the wavelength of the light, and the angle of incidence. The fraction of the light that is reflected increases with increasing angle of incidence θ_i [35]. Generally speaking, reflected light can be divided into two categories: specular reflection and diffuse reflection. Specular reflec-

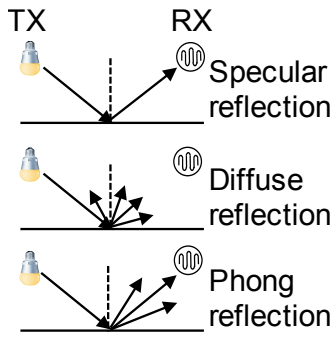

Figure 2.3: Types of reflections.

tor reflects all light which arrives from a given direction at the same angle, whereas diffuse reflector reflects that light in a broad range of directions. An example of the distinction between specular and diffuse reflection would be glossy and matte finishing. The latter has almost exclusively diffuse reflection, while the glossy cover has both specular and diffuse reflection. Thus many mixed-type reflections (see Fig. 2.3) can be found, as materials are not pure. A piece of metal, for example, can exhibit a specular or diffuse reflection if its surface has been polished or not.
More formally, let us consider the basic largely diffuse Phong reflection model, an empirical model of the local illumination of points on a surface [74]. Let us consider a single light ray impinging on the surface of

a material whose reflection and shininess coefficients are denoted by ρ and n. Let β be the incidence angle of the emitter to the reflecting point P, and let θ be the angle between the direction of maximum reflection of the light and the direction pointing from the reflecting point P to the receiver. Let n be the shininess constant of the reflection material. This parameter increases with the material's shininess, namely, n is larger for the materials of more mirror-like. The amount of light irradiating from the impinging point P and going towards the direction of the receiver has to be identified. By denoting k_a as the line-of-sight component at P, and k_s and k_d as the fractions of the impinging light transformed into specular and diffused reflections, respectively, then the reflected light towards the receiver h_r under the basic Phong model is given by [74]:

$$h_r = k_a + \rho \cdot (k_d \cdot \cos\beta + k_s \cdot \cos^n \theta). \tag{2.1}$$

According to the Phong model eq. 2.1, for each light ray $i \in \mathcal{I}$, its corresponding reflection towards the receiver $h_{r,i}$ is given by:

$$h_{r,i} = k_a + \rho_i \cdot (k_{d,i} \cdot \cos\beta_i + k_{s,i} \cdot \cos^{n_i} \theta_i),\ i \in \mathcal{I} \tag{2.2}$$

where $\rho_i \in \{\rho_H, \rho_L, \rho_B\}$ and its value is chosen based on the material where the ray i is impinging on. $\rho_i = \rho_L$). Similar rules apply to n_i, $k_{d,i}$ and $k_{s,i}$. The angles β_i and θ_i are calculated based on the positions of the emitter and receiver. Given the contributions of each light ray i in eq. 2.2, and the free path loss model for propagation to account for signal attenuation, the total receiver signal is calculated by summing up the contributions of all rays $i \in \mathcal{I}$.

2.1.3 Intensity Modulation with Direct Detection

LEDs emit incoherent light[2] allowing the usage of an Intensity Modulation (IM) scheme where the transmitted signal is modulated into the LED's instantaneous optical power [73]. In particular, non-negative input signals at the transmitter modulate the intensity of the emitted wave, since phase control of the optical carrier is not possible with incoherent light sources such as LEDs. In the receiver, a photodetector (PD) is used to convert the incident optical intensity into an output current signal, essentially linearly with

[2]Photons have different wavelength and phase, unlike coherent light sources such as lasers.

the received number of photons. At the transmitter the radiant intensity is controlled by the forward current through the LED, and must be in the operating region within the linear portion of V-I curve. Fig. 2.4 shows the ideal current-output modulation behavior under constant bias. Ideally, an

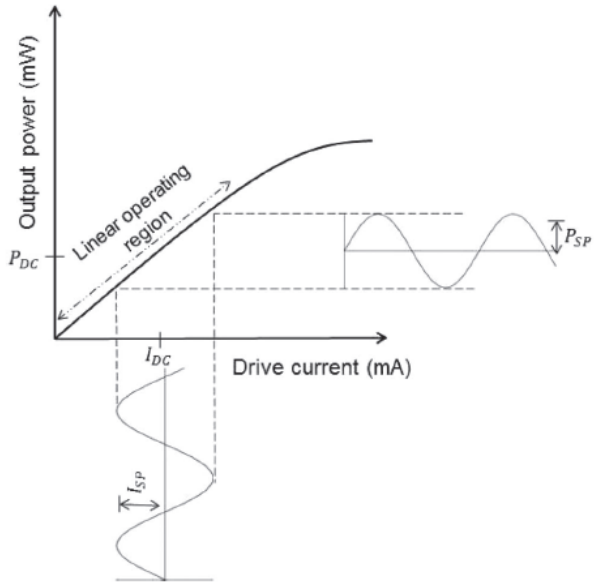

Figure 2.4: Intensity Modulation behavior [73].

input current I_{LED} with constant DC bias current I_{DC} and current swing I_{SP} can be expressed as

$$I_{LED} = I_{DC} + I_{SP}. \tag{2.3}$$

This would produce an output optical power of

$$P_O = P_{DC} + P_{SP}. \tag{2.4}$$

Since IM changes the instantaneous power of the LED, Direct Detection (DD) is the only feasible down conversion method. DD uses a photodiode to convert the incident optical signal power into a proportional current. Fig. 2.5 shows a general VLC link structure for an IM/DD based VLC system. The optically modulated signal waveform, $I_{t,sig}$ and average DC level, I_{DC} are

superimposed using a bias tee as shown in equation 2.3. The driving signal, I_{LED} is used to drive the LEDs which converts the electrical signal into intensity modulated optical signal. The light with optical power, P_O travels across the optical channel and is passed through an optical filter and is focused onto the PD by a focusing lens (if necessary). At this stage, the PD converts the optical signal back to the electrical signal. Noise adds up to the system at this level which are comprised of thermal and shot noise[3]. The received photo-current, I_{rec} is then amplified which is followed by signal processing and demodulation to retrieve the transmitted data [73].

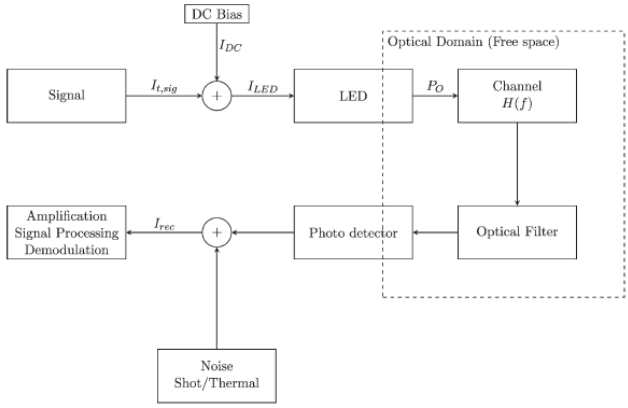

Figure 2.5: Intensity Modulation with Direct Detection scheme [73].

2.2 IEEE 802.15.7 standard brief introduction

The IEEE 802.15.7 Visible-light communication Personal Area Network (VPAN) standard describes the use of VLC for Wireless Personal Area Networks (WPAN) and covers topics such as network topologies, addressing, collision avoidance, acknowledgement, performance quality indication, dimming support, visibility support, colored status indication and color-stabilization. Moreover it provides (i) access to several hundred THz of unlicensed spec-

[3]Thermal noise is the electronic noise generated due to thermal agitation of charge carriers inside a conductor, whereas photon-generated shot noise is induced by ambient light.

trum; (ii) immunity to electromagnetic interference and noninterference with RF systems; (iii) additional security by allowing the user to see the communication channel; and (iv) communication augmenting and complementing existing services (such as illumination, display, indication, decoration, etc.) from visible-light infrastructures.

2.2.1 Scope

The standard defines a PHY and MAC layers for short-range optical wireless communications using visible light in optically transparent media. The visible light spectrum extends from 380 nm to 780 nm in wavelength. The standard is capable of delivering data rates sufficient to support audio and video multimedia services and also considers mobility of the visible link, compatibility with visible-light infrastructures, impairments due to noise and interference from sources like ambient light and a MAC layer that accommodates visible links. The standard also adheres to applicable eye safety regulations [1].

2.2.2 PHY and MAC layers

The PHY layer supports multiple PHY types, as follows [1]:

- PHY I: this PHY type is intended for outdoor usage with low data rate applications. This mode uses On-Off Keying (OOK) and Variable Pulse Position Modulation (VPPM) with data rates in the tens to hundreds of kb/s, depending on the modulation and the coding defined in the standard;
- PHY II: this PHY type is intended for indoor usage with moderate data rate applications. This mode uses OOK and VPPM with data rates in the tens of Mb/s, depending on the modulation and the coding defined in the standard;
- PHY III: this PHY type is intended for applications using Color-Shift Keying (CSK) that have multiple light sources and detectors. This mode uses CSK with data rates in the tens of Mb/s, depending on the modulation and the coding defined in the standard.

The IEEE 802.15.7 standard maps the intended applications to three topologies: peer-to-peer, star, and broadcast, as shown in Fig. 2.6.

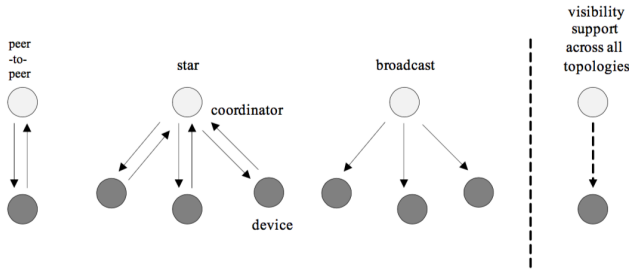

Figure 2.6: Supported MAC topologies [1].

In the star topology, the communication is established between devices and a single central controller, called the coordinator. In the peer-to-peer topology, one of the two devices takes the role of coordinator. The network formation is performed by higher layers, but they are not part of the standard.

2.2.3 Security

From a security perspective, IEEE 802.15.7 VPAN is slightly different from other wireless networks, due to directionality and visibility. In fact, because of its characteristics, if an unauthorized receiver is in the path of the communication signal, it can be recognized. Also, the signal will not travel across medium such as walls, unlike RF-based wireless networks. However, security algorithms are still provided in the standard for features such as data confidentiality, authentication and replay protection [1]. Devices can be low-cost and have limited capabilities in terms of computing power, available storage, and power drain. Communications cannot rely on the online availability of a fixed infrastructure and might involve short-term engagements between devices that may never have previously communicated. These constraints limit the choice of cryptographic algorithms and protocols and influence the design of the security architecture because the establishment and maintenance of trust relationships between devices need to be addressed with care. In addition, battery lifetime and cost constraints can put severe limits on the security overhead these networks can tolerate [1]. The cryptographic mechanism in the standard is based on symmetric-key cryptography and uses keys that are provided by higher layer processes.

2.3 Challenges

VLC is gaining a lot of attention because the advantages and the peculiarities the technology has. However the research community has still to face some big important challenges and to give effort for solving them, making VLC an affordable and reliable mean of communication. To date, as the state of the art, the most crucial open points are the following:

- lack of a well defined uplink method;
- interference analysis (natural and artificial sources);
- channel modeling and multipath effect analysis.

Even if an InfraRed (IR) connection is often used as uplink, this solution limits a lot the responsiveness and the range of the communication [12, 18]. A very few papers reported the usage of LEDs for both emission and detection, ensuring a bi-directionality [27], [82]. Another relevant option is the usage of mixed Wi-Fi and VLC system, where one technology compensate the lacks of the other [14, 16, 69]. A few papers analyse the interference generated by natural and/or artificial sources. Finally, a proper channel model is still lacking for both indoor and outdoor communication. IEEE 802.15.7 refers to simple case studies [1] for indoor, whereas for outdoor, most of the work is based on simulation analysis [54] and a very few investigate realistic scenarios [13, 81].

Chapter 3

Visible Light Communication for vehicular applications

In this chapter the importance of using wireless communications in vehicular environments and future intelligent automotive sectors is presented and discussed. Along the chapter VLC systems are compared with radio-frequency techniques, by analysing advantages, challenges and direction of future work. Moreover a brief introduction of the IEEE standard suite for vehicular communication is given.

3.1 Intelligent Transportation Systems introduction

The number of automobiles that use the transportation infrastructure is constantly increasing. Within this context, the number of victims resulting from traffic accidents is also increasing, making road accidents one of the leading causes of death [71]. The scientific community, the automotive industry and the governmental agencies are joining their efforts to increase the safety of vehicles and roads. This effort have led to a new paradigm: "help people avoid accidents" instead of the old one "help people survive accidents". With the advent of self-driving cars, a reliable communication infrastructure is needed also for achieving more efficiency in transportation systems. For example, a traffic management could be implemented exploiting a commu-

nication among road infrastructure and vehicles. Vehicular communications are divided mainly into two branches:

1. Infrastructure-to-Vehicle (I2V) or Vehicle-to-Infrastructure (V2I) communications;

2. Vehicle-to-Vehicle (V2V) communications.

Intelligent Transportation Systems (ITS) involves the application of the advanced information processing, control technologies, sensors, and communications in an integrated approach to improve the functioning of the road transportation systems. Generally speaking, ITS considers using state-of-the-art cooperative technologies in order to reduce the number of accidents and of associated fatalities. It also aims at improving efficiency in transportation system, e.g. reducing the CO_2 emissions. Moreover, this kind of system adds value to the transportation system by providing real-time access to relevant traffic information. By using I2V/V2I and V2V communications, ITS continuously collects traffic data, analyzes it and distributes it, in order to increase the vehicle awareness. Furthermore, this information enables an efficient management of the transportation system, increasing efficiency and reducing traffic jams. A system like this requires a specific deployment of intelligent infrastructures able to collect data and process it. Of course the biggest challenge is to maintain the implementation cost as low as possible without lack of reliability.
Considerable efforts have been made in the last decade by researchers from both academia and industry to enable the cooperative ITS, which is seen as the next generation of ITSs and it is enabled by V2V and V2I communications. Worldwide efforts in this area include cooperative ITS research programs[1]. The IEEE has also developed a standard for radio communication systems, known as the Wireless Access in Vehicular Environments (WAVE), to provide interoperable wireless networking services for transportation [80].

Vehicular VLC oriented standard Even if IEEE has not released a proper standard for Vehicular VLC (V^2LC) yet, the IEEE 802.15.7 includes a

[1]Vehicle Safety Communications (VSC), Crash Avoidance Metrics Partnership/VSC-2, and IntelliDrive run by the U.S. Department of Transportation, the PATH program lead by the University of California, Berkeley, CAR2CAR Communication Consortium, COMeSafety2, Drive C2X, iTETRIS, AKTIV, and eImpact projects in Europe, and SmartWay in Japan among others [80].

PHY layer type for outdoor communication (PHY-I, as reported in Sec. 2.2.2) which could regulate vehicular systems. It has a lot of limitations, and it is not properly meant for this kind of environments [22]. A new dedicated standard for vehicular applications should be very strict concerning the robustness to perturbations and to latencies. In order to do that, a proper standard should further simplify the frame structure, for reducing the overhead and enhance the throughput. Other aspects that should be approached are related to the message generation rate and to vehicular-specific networking. Here, the standard should provide information referring to dynamic mesh topologies, able to provide rapid and efficient channel access [22]. A gratifying aspect concerning the future development of the VLC technology is the fact that a revision of the standard, known as IEEE 802.15.7r1, is now under development. This revised version includes vehicular communications as a fundamental VLC use case, mentioning here V2I and V2V applications. In this case, the standard considers the requirements of vehicular communications and aims to enhance mobility, data rates, robustness, and to enhance the networking protocols [22].

3.2 IEEE Wireless Access in Vehicular Environments standard brief introduction

Dedicated Short-Range Communications (DSRC) is a suite of standards that aim at the exchanging of vehicular safety messages. Also referred as "Wireless Access in Vehicular Environments" (WAVE) (both acronymous are indistinguishable used), is a radio communication system intended to provide seamless, interoperable services to transportation. These services include those recognized by the U.S. ITS architecture and many others contemplated by the automotive and transportation infrastructure industries around the world, such as communications between vehicles and infrastructure, and communications among vehicles [2]. WAVE is meant to be used in conjunction with the family of IEEE 1609.x standards that are focused on MAC and network layers. It is quite complex and is built over the IEEE 802.11.p standards by amending many tweaks to guarantee fast reliable exchange of safety messages. A DSRC network is built over two basic units: Road-Side Unit (RSU) and On-Board Unit (OBU). The RSU is a stationary unit that connects roaming vehicles to the access network, which is connected to a backbone network. The OBU is a network device fixed in a roaming vehicle

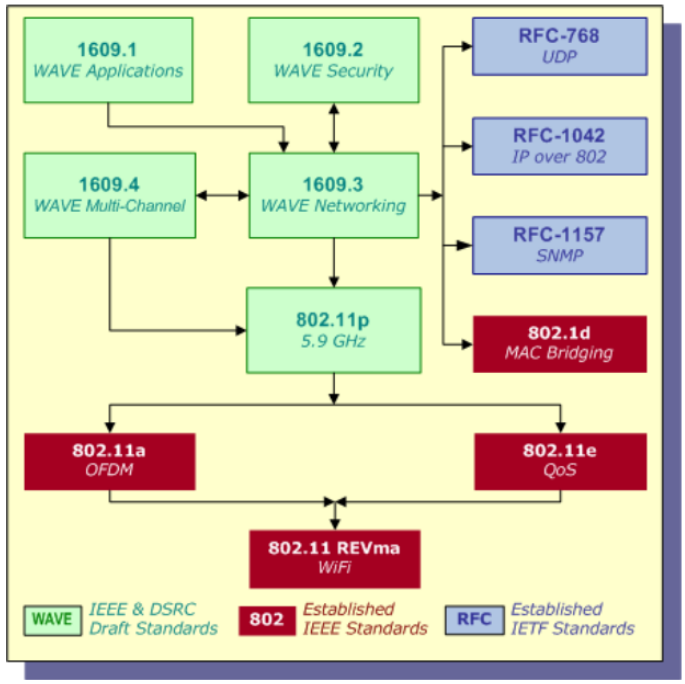

Figure 3.1: Simplified DSRC Standards suite [66].

and is connected to both the DSRC wireless network and to an in-vehicle network. The wireless connection between RSU and OBU is based on WAVE standards suite shown in Fig. 3.1. As OBUs move between communication zones, vehicles exchange information with the roadside. In addition, vehicles use the same WAVE media to communicate with each other [66].

3.3 Advantages and challenges

As Tab. 3.1 shows, VLC is well positioned to address both the low latency required in safety functionalities (e.g., emergency messages, intersection collision warning or platooning) and high speeds required in so-called infotainment applications (e.g., map, media and updates downloads, point of interest notifications). One of the strongest advantages of VLC is its low complexity and the reduced implementation cost. Being already half integrated in the existing transportation infrastructure, as well as in vehicle lighting systems, make VLC an ubiquitous technology and could allow a fast market penetration. Moreover communication bi-directionality is, even if not trivial, quite straightforward since modern vehicles have already LED-based illumination systems, both on the front and on the back.
Automotive applications don't need high throughput, but larger distances need to be achieved. As several indoor implementations report, this tradeoff is possible. In fact, high speed connections drop their data rates as far as the receiver is placed. However, if communication-based vehicle safety applications are considered, this use case requires very high Packet Delivery Ratio (PDR) and latencies as low as 20 ms, meaning that a higher robustness to disturbances is expected [20]. VLC is also appealing for vehicular scenarios in which the use of a RF band is restricted or banned due to the safety regulations (e.g., oil/gas/mining industries, and military vehicle platoons). Another attractive feature of VLC is the positioning and navigation capabilities. Since Globral Positioning System (GPS) fails to provide a sufficient accuracy in environments where there is no LOS paths such as tunnels or urban canyons, VLC-based positioning systems could be used to complement the accuracy exploiting the lighting fixtures. A resolution error of up to of tens of centimeters, obtained with VLC, outclasses a typical positioning error of up to 10 m associated with the GPS. This could pave the road to a much more reliable vehicle safety applications. Of course, V^2LC also has many challenges to overcome. Here a list of the most important:

Table 3.1: Comparison of IEEE 802.15.7 and 802.11.p standards [80].

Type	**802.15.7**	**802.11.p**
Communication mode	P2P (LOS or diffuse)	P2M / broadcasting
Latency	Very low	$< 50ms$
Data rate	Up to 400 Mb/s	Up to 54 Mb/s
Range	Up to 100 m (single hop)	Up to 1 km
Frequency band	400-790 THz	5.8-5.9 GHz
License	Unlicensed	Licensed
Cost	Low	High
Mobility	Medium	High
EMI	No	Yes
Power consumption	Relatively low	Medium
Coverage	Narrow	Wide
Weather conditions	Sensitive	Robust
Ambient light	Sensitive	Not affected

- communication range need to be increased;
- robustness to weather conditions, sunlight and ambient light;
- mobility of devices has to be studied and enhanced;
- visible light positioning algorithms need to be improved;
- parallel visible light communications have to be developed in order to increase the reachable distance and maximum rate;
- RF and VLC systems should be integrated in unique networks in order to be as much ubiquitous as possible.

3.4 Contributions

In this dissertation, the following V^2LC contributions are presented:

1. an outdoor vehicular link characterization (I2V VLC system) proposal which exploits an LED-based traffic light for communicating with vehicles, which is described at Chapter 5;
2. a simple, preliminary, VLC propagation model proposal based on experimental measurements, which is detailed in Sec. 5.3;
3. an IEEE 802.15.7 PHY-I complaint, low-cost transceiver design and first implementation, which is detailed in Sec. 5.4.

Chapter 4

LED-based Positioning Systems

This chapter introduces LED-based Positioning Systems (LPS) and discusses the potentials of this technology with respect to traditional radio-based techniques. A positioning system based on a single LED, chosen as a case study for this dissertation, is introduced and its algorithm fully described.

4.1 Introduction

Positioning systems used for the purpose of estimating user location are the basis for navigation-based services. As the present mainstream in positioning systems, GPS is widely used in aircraft, vehicles, and portable devices in order to provide real-time positioning and navigation. However, in challenging environments, such as urban canyons and indoors, GPS positioning and navigation is inaccurate and discontinuous since the signals transmitted by satellites are usually degraded and interrupted by clouds, ceilings, walls, and other obstructions. A hot topic in the positioning service is the "last meter" problem, in that indoor applications require much more accurate positioning than outdoor applications. Consequently, Indoor Positioning Systems (IPS) using indoor wireless signals (WiFi, Bluetooth, RFID, etc.) have been proposed to fill the gap of GPS signals to improve the performance of indoor positioning. Over the last few decades, these signals have been employed in IPS technologies, among which WiFi and Bluetooth positioning systems are mostly utilized and which have already been widely deployed in current smart devices. LED-based positioning systems (LPS) emerged in recent

years, which leverages visible light signal instead of radio frequency. Over the past few years, many algorithms for LPS have been proposed and verified by experiments. LPS have shown to be more accurate (0.1-0.35 m positioning error) when compared to WiFi (1-7 m), Bluetooth (2-5 m), and other technologies [40]. Furthermore, some systems have achieved millimeter-level positioning accuracy [45, 68].

4.2 Advantages and challenges

Compared with other systems mentioned before, LPS have the following advantages:

- they can be used in indoor spaces where GPS doesn't work;
- they can be installed inexpensively since they utilize existing lighting systems with very few modifications applied;
- the precision of visible light positioning is higher than traditional positioning. For example, the research shows that the number of LED luminaries is ten times more than Wi-Fi in a typical indoor building [59], which contributes to the higher accuracy;
- they can be used in RF sensitive areas like hospitals and air crafts because it does not generate RF interference.

Since the beginning of investigation in this field is quite recent, LPS have many challenges to face as well. Here some of them can be cited:

- as well as in general VLC systems, the lack of a channel model limits the complete understanding of the real capabilities the technology has;
- the performance of current LPS is limited by the demodulation bandwidth of VLC, especially for multi-source scenarios. Here, the multipath transmission is extremely challenging for IPS receivers with limited processing capability, such as "complementary metal oxide semiconductor" (CMOS) cameras;
- technically, the receiver only senses the light lobes within its field-of-view; therefore, a receiver with a wider FOV is used for a large-scale indoor environment. A wider FOV, however, results in receiving more undesired signals from Non-Line-Of-Sight reflections or ambient light,

which may lead to performance degradation. Hence, a trade-off needs to be made for the choice of FOV in the IPS design [59];

- because Signal-to-Noise Ratio (SNR) is essential to evaluate the performance of the VLC systems, the noise in a LPS should not be neglected. Many LED IPSs report large positioning errors (above 0.4 m) in the outer region, i.e., outside the area surrounded by the LEDs, or marginal area [59]. This is mainly because the light power received from far-off LED transmitters is largely degraded by the long distance travel and a large irradiance angle, which is quite comparable to the noise and leads to a relatively low SNR in the area;

- since LED is an illumination source, luminous fluxes are dispersed in the environment. This creates reflecting components from the walls, ceilings, tables, mirrors, and any other surfaces around. Although the reflecting components are much weaker than the LOS channel, due to multipath effect, they are still perceptive to the optical sensor and may contribute to a diffuse channel in the VLC system which will influence SNR, "Bit Error Rate" (BER), and other system performance metrics. Most of the LPS perform an Received Signal Strength (RSS) based positioning by transferring received light power to distances. Therefore, the distance estimation will become worse if the reflected components are mixed into the received signals, leading to a larger positioning error [89].

4.3 An LPS case study

In the following section a brief description of a relative two-dimensional positioning system [36] and of the platform it uses, are given. The full system is exploited in Chapter 6 and it is taken as a case study for analysing the effect of multipath on a LPS.

4.3.1 OpenVLC platform

OpenVLC is a general-purpose software-defined platform for networked VLC. The node is built around the BeagleBone Black (BBB) board [4] a cost-effective, user-friendly, versatile single-board computer with a small form factor. OpenVLC consists of a BBB board, a VLC front-end transceiver,

and a software-defined system implementation. The front-end transceiver adopts a single LED together with a few basic electronic components for both transmission and reception (see Fig. 4.1). OpenVLC's software components are implemented as a Linux driver that communicates directly with the LED front-end and the Linux networking stack. As a result of this design choice, the VLC communication interface can take advantage of the vast range of Linux tools. The communication between two OpenVLC nodes is illustrated in Fig. 4.2 [7] The software-defined transmitter (TX) selector can

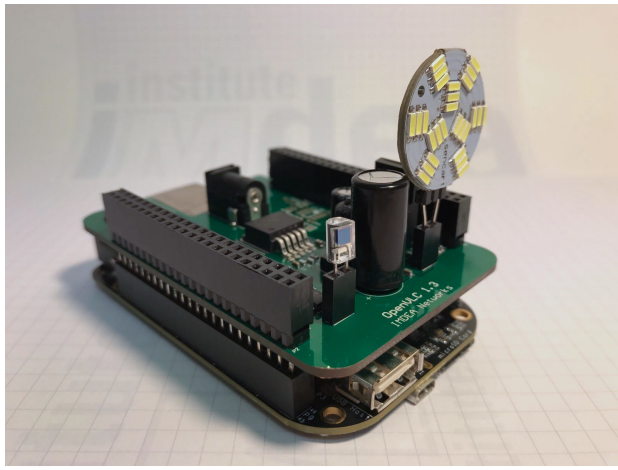

Figure 4.1: OpenVLC board.

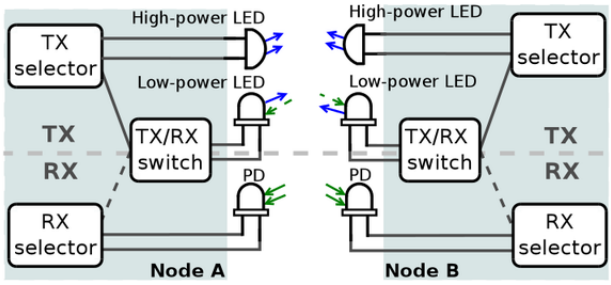

Figure 4.2: OpenVLC system - block scheme [7].

choose the TX between a low-power LED and a high-power LED. Similarly, the software-defined receiver (RX) selector can select as a receiver between a

PD and a low-power LED (working as a sensor). The communication stack of OpenVLC is illustrated on the left of Fig. 4.3. Primitives are implemented to build various PHY and MAC layer protocols in the Linux operating system.

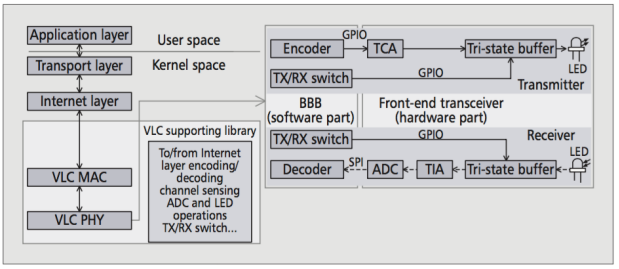

Figure 4.3: OpenVLC system - communication stack [82].

TX, RX, and TX/RX switching In TX mode, the BBB outputs the signal to the anode of LED for a symbol period. In RX mode, the small photo-current is amplified by the TIA (Trans-Impedance Amplifier), and then sampled by the ADC and converted into a digital signal. The BBB samples the output of the ADC at a fixed interval equal to one symbol period. The RX samples the output of ADC and stores the value in a sequence that will be decoded by the driver at a later time. The LED can be used as a TX and RX at the same time, so it can switch between those two modes through the software-defined that runs on the BBB.

Modulation and detection Intensity modulation for data transmission is used. Binary information is mapped to the presence (symbol HIGH) or absence (symbol LOW) of the visible light carrier. At the transmitter, the on-off keying (OOK) modulation and the Manchester Run-Length Limited (RLL) code are used. At the receiver, demodulation is performed with direct detection (DD). Based on the measured voltage, the receiver detects a received signal as a sequence of symbols HIGH and LOW that are then converted to binary data.

Preamble The PHY layer transmits each frame with a fixed-length preamble, consisting of an alternate sequence of HIGH and LOW starting with a

HIGH symbol. The numbers of HIGH and LOW symbols in the preamble are the same. To convert symbols into binary data, an adaptive symbol detection threshold is adopted because the received light intensity is greatly affected by the free path loss attenuation of light transmitted from the TX to the RX. This detection threshold is obtained on a per-frame basis by averaging out the digital samples of the preamble sequence. A special frame delimiter (SFD) field is appended to the end of the preamble.

Frame format The frame format is shown in Fig. 4.4. If the frame has no payload (length = 0), it is inferred to be an ACK. Otherwise, it is a DATA frame. Each frame can carry a payload from 0 to MAX (a predefined value) bytes. The destination and source addresses follow the Length field, and each occupies 2 bytes. The 2-byte Protocol field identifies the upper layer protocol encapsulated in the frame pay-load. A two-byte cyclic redundancy check (CRC) over the MAC header and payload is appended after the payload. The Reed-Solomon (RS) error correcting code is appended to the end of each frame.

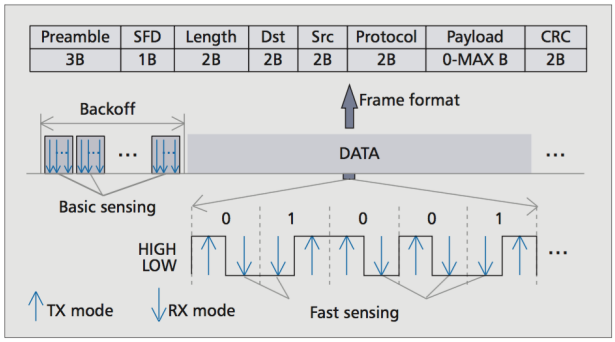

Figure 4.4: OpenVLC system - frame composition [82].

4.3.2 Relative two-dimensional positioning system

Consider two nodes[1], A and B, where node A wants to know the relative position of node B with respect to its position. The aim of the system is: as long as a node is within the illumination coverage of a neighbor, the node

[1]Nodes could be any object containing a single light such as motorbikes or robots.

should be able to obtain its relative position without any prior knowledge of its surroundings. These relative positions could be used for safe driving in the case of motorbikes or for task coordination in the case of robots [36].

Consider an LED light source (transmitter) and an optical receiver, as illustrated in Fig. 4.5. Given any output power at the transmitter (LED), the received signal strength at the receiver (PD) depends on three key parameters: the distance between them (d), the irradiation angle (ψ) and the incidence angle (θ). The longer the distance, or the wider any of these angles, the lower the RSS. The interplay among these three parameters leads to Lambertian radiation patterns, where the maximum length of the coverage is mainly determined by the output power of the LED and the maximum width is determined by the Lambertian order (m). A small value of m leads to a broad coverage of the LED; a large m leads to a long but narrow coverage.

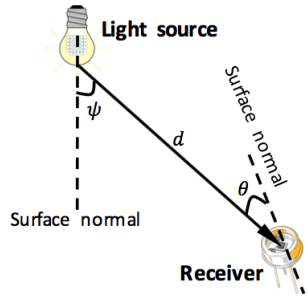

Figure 4.5: Propagation properties of LEDs [36].

Formally, this pattern is captured by the well-known Lambert's cosine law:

$$R_t(\psi) = \frac{m+1}{2\pi} cos^m(\psi). \tag{4.1}$$

The channel loss H(0) between the transmitter and receiver

$$H(0) = A_{RX} \cdot \frac{m+1}{2\pi d^2} \, cos^m(\psi) \cdot cos(\alpha) \tag{4.2}$$

where A_{RX} is the sensing area of the photodiode of the receiver, and Θ_c is the PD's field-of-view.
Letting P_t and P_r denote the optical transmission power of the LED and the received power at the PD, respectively; and letting N refer to the sum of

ambient noise and the PD's shot and thermal noise; then P_r can be written as:

$$P_r = P_t \cdot H(0) \cdot g_r(\theta) + N \tag{4.3}$$

where $g_r(\theta)$ is the optical gain of the PD. $g_r(\theta)$ is a non-zero constant when $\theta \in [0, \theta_c]$, and is zero otherwise. Therefore, g_r is used to denote $g_r(\theta)$ in the calculation of P_r.

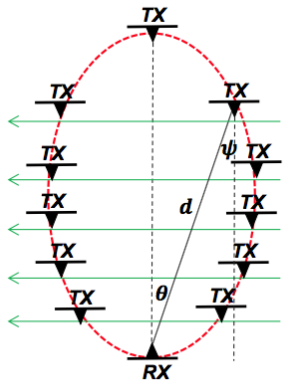

Figure 4.6: Iso-contours of received power [36].

Basic location principle Given a received power P_r, the TX can be located in multiple positions with respect to the RX. By referring to Eq. 4.2, for example, for a low P_r, the TX can be far away but aligned to the RX ($\psi = \theta = 0$), or it can be nearby but misaligned. If the TX orientation is fixed and it moves at different perpendicular distances from the RX, as illustrated in Fig. 4.6, each distance provides two locations where the received power is measured as P_r. All these locations form an iso-contour where the received power is the same. The principle behind the algorithm is to exploit changes in the iso-contours due to nodes' movements, see Fig. 4.7. If the RX rotates, the iso-contour changes from its original shape (red) to a new shape (blue). In this particular case, the change in the iso-contour is caused by the change in the incidence angle θ. The intersection of these two iso-contours can be used to estimate the relative position of the TX. Consider a system of two mobile nodes: one acts as a reference point (referred as receiver) that has a PD; and the other is a target to be localized (referred as transmitter) that has an

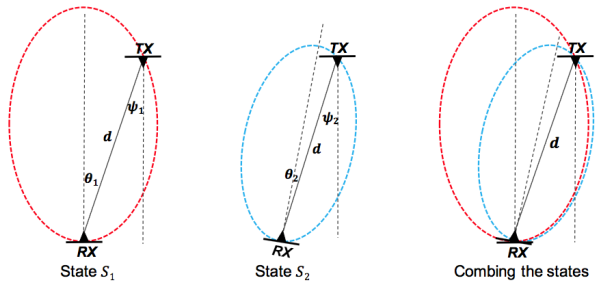

Figure 4.7: Localization using iso-contours intersection [36].

LED light source. Both nodes can measure their orientations and movement through on-board sensors, compasses and accelerometers respectively. The transmitter has information of the optical properties of its LED lights, such as the transmission power and Lambertian order. The transmission power and Lambertian order together with the transmitter real-time orientation are shared with the receiver via visible light communication. The receiver can decode the transmitted information through its PD and it can also measure the received power. Since it is assumed that both nodes are mobile, a state of the system S can be defined as follows:

$$S = (\alpha_{tx}, \alpha_{rx}, d, P_r) \tag{4.4}$$

where α_{tx} and α_{rx} are the orientations of the transmitter and receiver with respect to North, respectively, d is the relative distance of the transmitter with respect to the receiver, and P_r is the received power at the receiver. Assuming that the system is currently in state $S_1(\alpha^1_{tx}, \alpha^1_{rx}, d_1, P_1)$, then according to Eq. 4.3, the received power P^1_r for state S can be written as follows:

$$P^1_r = P_t A_{RX} \frac{m+1}{2\pi(d_1)^2} cos^m(\psi_1) cos(\theta_1) \cdot g_r + N. \tag{4.5}$$

A similar equation can be derived for a later state $S_2(\alpha^2_{tx}, \alpha^2_{rx}, d_2, P_2)$, where the relative position and the orientations of the transmitter and receiver change, and they are denoted by d_2, α_2, and α_2, respectively. So the measured received power is P^2_r:

$$P^2_r = P_t A_{RX} \frac{m+1}{2\pi(d_2)^2} cos^m(\psi_2) cos(\theta_2) \cdot g_r + N. \tag{4.6}$$

In the above two equations, we have six variables: the irradiation angles ψ_1, ψ_2, the incidence angles θ_1, θ_2, and the relative distance d_1 and d_2 between the transmitter and receiver. So they cannot be solved directly. To overcome the aforementioned challenges some hypothesis are stated:

1. nodes are forced to broadcast continuously and periodically their orientation and LED parameters via visible light communication. And, at the receiver, we only consider changes in orientation detected within a very short period of time, so we can assume that the locations of the TX and RX remain "constant". It reduces the number of variables in the above equations from six to five, because over a short period of time we can assume that $d_1 = d_2 = d$.

2. the information coming from the compasses are exploited to derive dependencies among the five remaining variables, allowing the identify of a single solution in most cases.

After some dependencies calculation (refer to [36]) and substituting them into Eq. 4.5 and 4.6, the following equation system is obtained:

$$P_r^1 = P_t A_{RX} \frac{m+1}{2\pi(d)^2} cos^m(\psi_1) cos(f(\alpha_{tx}^1, \alpha_{rx}^1, \psi_1) \cdot g_r + N \tag{4.7}$$

$$P_r^2 = P_t A_{RX} \frac{m+1}{2\pi(d)^2} cos^m(g(\alpha_{tx}^1, \alpha_{tx}^2, \psi_1) cos(f(\alpha_{tx}^1, \alpha_{tx}^2, \alpha_{rx}^1, \alpha_{rx}^2, \psi_1) \cdot g_r + N. \tag{4.8}$$

In these two equations there are only two unknowns (ψ_1 and d), and thus, they can be solved numerically.

Variable distances Until know, the analysis has focused solely on events where rotations are expected. But some mobile scenarios may not have any rotations. For example nodes moving on a straight path at variable speeds will not change their orientations, but their relative distances will change. For these types of scenarios, the equations describing the system at states S_1 and S_2 are

$$P_r^i = P_t A_{RX} \frac{m+1}{2\pi(d_i)^2} cos^m(\psi) cos(\theta) \cdot g_r + N \tag{4.9}$$

with $i \in (1, 2)$. If the difference in distances between states S_1 and S_2 is assumed that can be estimated (by, for example, performing a double

integral of an accelerometer):

$$\varepsilon = d_2 - d_1 \tag{4.10}$$

then, based on Eq. 4.9 and Eq. 4.10, a closed-form expression for the relative distance is obtained as follows:

$$d_2 = \varepsilon / \left(1 - \sqrt{P_r^2 / P_r^1}\right). \tag{4.11}$$

After some substitutions (refer to [36]), the following expression is reached:

$$\frac{2\pi d_2^2 P_r^2}{(m+1)A_{RX}} - N = cos^m(\theta + \pi + \alpha_{tx} - \alpha rx)cos(\theta) \tag{4.12}$$

where θ can be calculated numerically. An important point to consider for these no-rotations cases is that the relative location is no longer obtained by intersecting two Lambertian iso-contours, but by intersecting a single Lambertian iso-contour and a circle. This implies that unless the TX and RX are aligned ($\psi = \theta = 0$), two possible locations are always obtained. In this case the system reduces its accuracy to one dimension distance.

Implementation The localization algorithm is implemented on the OpenVLC platform 4.3.1. The platform is customized to satisfy the requirements of the localization technique. The system functional block scheme is shown in Fig. 4.8. To run the localization method, the following information from the TX are needed: transmitted power, Lambertian order m of its transmitting LED and its orientation; and these from the RX: received power and its orientation.

Measuring the relative positions Orientation plays a crucial part in the system and it can be measured by inertial sensors. The sensor used is Adafruit 9-DOF Absolute Orientation IMU Fusion Breakout - BNO055, which does sensor fusion of the magnetometer and accelerometers for higher accuracy. OpenVLC node communicates to the sensor using the serial port, as shown in Fig. 4.9. The sampling rate of the sensors is equal to 500 Hz.

The transmission power, Lambertian order of the LED at the TX, and the TX orientation are shared with the RX through VLC. In order to have controlled environment for our evaluation, measurements are done in a dark environment without external light sources. The localization algorithm is implemented to operate in real time, with interactions among the blocks

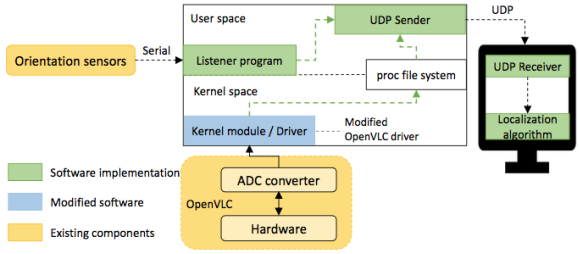

Figure 4.8: Functional blocks of LPS case study [36].

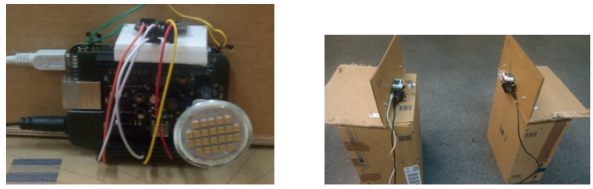

Figure 4.9: Hardware used in the implementation [36].

illustrated in Fig. 4.8. Raw power readings from the data frame preamble are collected and shared with the user space. A listener program collects the orientation information from sensors by continuously polling the serial port in the BBB board. The listener thread then sends the data to the computer every second using UDP. In the computer, a program reads the UDP messages and every two messages, runs the localization algorithm based on Eq. 4.8.

Experimental evaluation - Relative distance variation Since at Chapter 6 only a distance variation movement is analysed, here, only the algorithm experimental evaluation of the relative distance variation is reported. In these experiments both the TX and RX are free to move assuming that they do not change their orientation with respect to each other. In order to compute the correct value of the system, the distance difference needs to be known as well as the received power. In these experiments the distance change is assumed to be known (in a real environment it can be estimated by performing, for example, a double integration of the accelerometer input). In the experiments, the distance between the TX and RX changes between the first and the second measurement with different steps (10, 20, 40, 50 cm). This is performed for different angles in degrees between the TX and RX (0, 20, 45, 60, -20, -45, -60). The results of the experiments are depicted in Fig. 4.10. The average distance errors in the x-axis and y-axis are both less than 2 cm.

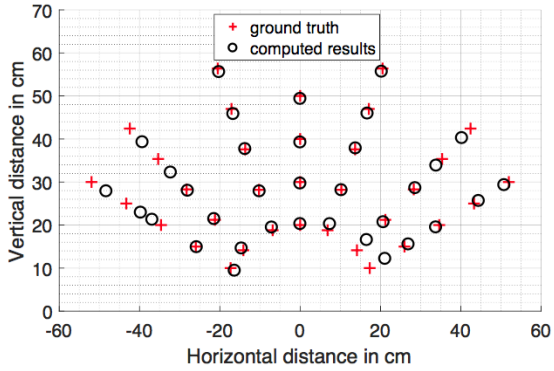

Figure 4.10: Accuracy results for distance changes [36].

4.4 Contributions

The main contribution of this thesis about LED-based Positioning Systems is an in-depth performance analysis of a relative positioning system (introduced in Sec. 4.3.2) in realistic scenarios. This study, performed at IMDEA Network Institute of Madrid during an 11-month internship, exploits a small scale mobile environment featuring OpenVLC platforms and different types of reflective object samples. The experimental campaign as well the data processing are detailed at Chapter 6.

Chapter 5

Infrastructure-to-Vehicle VLC link characterization with LED-based Traffic Light

This chapter presents the preliminary work that leads to an outdoor vehicular link characterization (I2V VLC system) proposal. It exploits a LED-based traffic light for broadcasting messages towards vehicles. In particular, a preliminary propagation study of a simple VLC system and a first IEEE 802.15.7 PHY-I complaint SDR VLC transceiver implementation are here introduced and detailed.

5.1 Proposal overview

The aim of this dissertation section is to present an outdoor vehicular link characterization (I2V VLC system) proposal. The main idea is to exploit a COTS LED-based traffic light for designing a VLC system able to send traffic and safety information towards vehicles. The system is also a mean to analyse the outdoor optical wireless channel in realistic scenarios (see Fig. 5.1). The link characterization is due to be done through an experimental campaign in which several scenarios and realistic conditions are deployed. In particular numerous distances and angles between the traffic light and a vehicle, and three different receiver onboard locations, are supposed to be

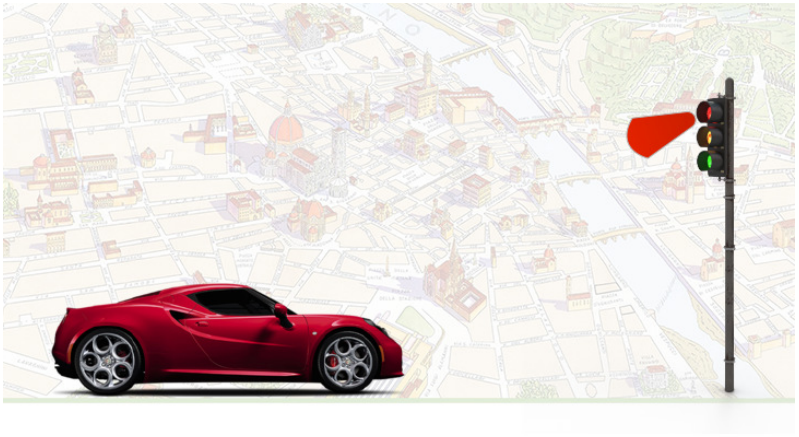

Figure 5.1: Infrastructure-to-Vehicle VLC system with LED-based Traffic Light.

experimented. As shown in Fig. 5.2 a grid of several positions along a two-lane road is considered, involving different distances and angles in which the received signal varies. Figure 5.3 presents the initial proposal of testing

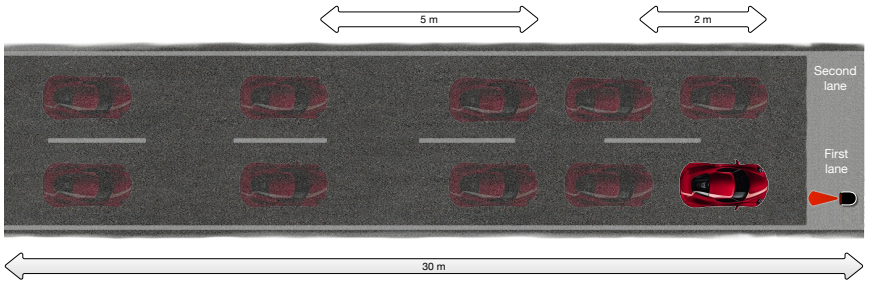

Figure 5.2: Experimental measurement setup - Distances and angles between traffic light and vehicle.

three locations onboard a vehicle: at headlamp, at wing mirror, at rear-view mirror. The optimal receiver location should be pinpointed. Further topics (e.g. a vehicle that acts as a relay and forwards messages towards a following vehicle for platooning systems) will be investigated during the experimentation that is supposed to be a future work as well as processing the acquired

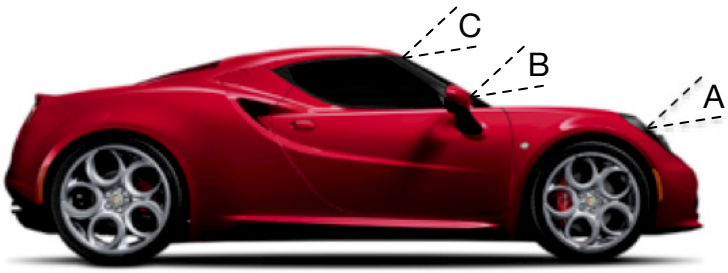

Figure 5.3: Experimental measurement setup - Receiver onboard locations.

raw data (refer to Chapter. 7) for study the multipath contribution. In the following, the preparatory work useful to deploy the aforementioned system is presented and detailed. In particular a preliminary propagation study of a simple VLC system and a first IEEE 802.15.7 PHY-I complaint SDR VLC transceiver implementation are described.

5.2 Related work

A few papers have already investigated a I2V system which involves a traffic light. In [11] a traffic information system using existing LED traffic lights is developed. It focuses on its visible rays and power used for traffic control, the number and location of the traffic lights, and the movement toward LED traffic lights. Authors design the best service area not to interfere with other service areas and analyse its basic performance such as the suitable modulation, required SNR and the amount of receivable information. A conceptual integration method of VLC into ITS along with reference model is presented in [51]. Some interesting experiment results show performances (BER and throughput) of a case study with different modulations.

Authors in [70] propose a road-to-vehicle visible communication system for ITS. In this system, a LED traffic light is used as transmitter and a photodiode is used as receiver. The paper focus on problems related to receiving

information from long distance and related to tracking the transmitter along a certain moving distance between a vehicle and the traffic lights. Imaging optics are applied for handling the communication over long distances. Two cameras are used to solve the relationship between the transmitter and the receiver position changes with time, and vibrational correction technique is also fixed to the system to minimize vibrational affections. Experiments have been conducted to confirm the proposals.

Often image sensor and image processing are used in outdoor VLC system, as in [28] and [83]. The performance of a LOS link in an empirical outdoor environment has been carried out in [28]. Possible interference in the LOS link is first characterized, including both background solar radiation and artificial light sources. The frequency response of COTS LED traffic light lamps as transmitter devices is then investigated, which reveals a modulation bandwidth up to 5 MHz for common LED traffic lights. Also the theoretical LOS path loss model is proposed and validated by the measurement results. Finally, the practical communication system performance based on the above characterization is evaluated, with results shown that a data rate of 1 Mb/s could be achieved at a distance of 75 m with a raw BER of 10^{-2} in the electronics noise limited case.

In [83] a receiving method for VLC with LED-based traffic lights using 2-D image sensor receiver is proposed. The maximum receiver field-of-view and the best vertical inclination are discussed. Authors analyzed and quantified the possible SNR improvement when different numbers of pixels are applied. Results indicate that using more pixels can increase the received SNR and the service area becomes wider compared to the conventional system using Avalanche Photodiode (APD) receiver. Then the optimum pixel number has been computed for accomplishing a reliable communication. Also in [44] proposes camera for detecting signal broadcasted by an LED traffic light. In this paper experiments in real-world environment verify the proposed algorithm, using the sequence captured by a high-speed camera (1000 fps) fixed on a vehicle moving straight at 30 km/h.

The aforementioned works don't take into account the effect of ambient-light noise which varies largely from day time to night time. Authors of [53] propose an analytical daylight noise model based on a modified blackbody radiation model to capture the effect of ambient-light noise and conduct an in-depth study on the impact of daylight on the system performance. The proposed daylight noise model allowed the authors perform an analytical

analysis which produces relatively accurate results with less complexity, as compared to the existing simulation. The authors also introduce a new receiver structure employing the selective combining technique to significantly reduce the effect of background noise, able to achieve an enough-reliable link and establish a stable communication link at any time of the day. [19] and [21] introduce receiver sensor and adaptive receiver sensor design intended for vehicular communication applications, also offering a review of the solutions found to mitigate the effect of the problematic conditions (distance and weather conditions).

Vehicle-to-Vehicle links are experimentally studied in [49] and [88] using, in the former, a critical weather condition like fog and, the latter a COTS headlamp. Both experimental results demonstrate that the proposed VLC-based V2V system offers a reliable V2V data transmission. Beside weather condition, another critical condition for V^2LC is the relative movement of vehicles. [50] proposes a motion modeling of VLC transmitter for image sensor based VLC receiver. All the three vehicular channel types (I2V, V2I, V2V) are investigated and simulated.

Dual channel communication between vehicles (i.e. full duplex V2V) is studied in [79]. This paper show the dependency of the received optical power of single channel VLC on the angle and distance, and demonstrate that Lambertian model does not represent the automotive LED fog light radiation pattern accurately. Then it demonstrates that dual channel usage increases the angular limitation by up to 10° compared to the single channel VLC. Also authors show that dual channel improves the packet delivery error rate performance at only short distances due to the photodiode (PD) saturation led by light intensity overlapping at higher distances.

5.3 Preliminary propagation model study

In this section a propagation model of a simple visible light system through an experimental measurement campaign is presented [67]. The scope is to come up with a fine tuned propagation model which also accounts for reflections from the optical bench. The experiments were conducted in the European Laboratory of Non Linear Spectroscopy (LENS) of Sesto Fiorentino (Florence, Italy).

5.3.1 Test description

A measurement campaign is performed in order to study a simple indoor VLC transmission channel. A 3W LED green light Epistar WX-PAXG851A3 is used as a fixed transmitting source, whereas a Vishay BP34W photodiode is exploited as a photodetector and moved around on an 80-location measurement grid (a 1200 × 900 mm optical bench enclosed by black walls). A counter-polarization circuit, a transimpedance stage and a low-noise amplifier completes the receiving chain. Each measurement position is 100 mm far from another in both directions (X-axis and Y-axis). Since the photodetector has a fixed orientation angle, it always faces the short side of the bench (see Fig. 5.4).

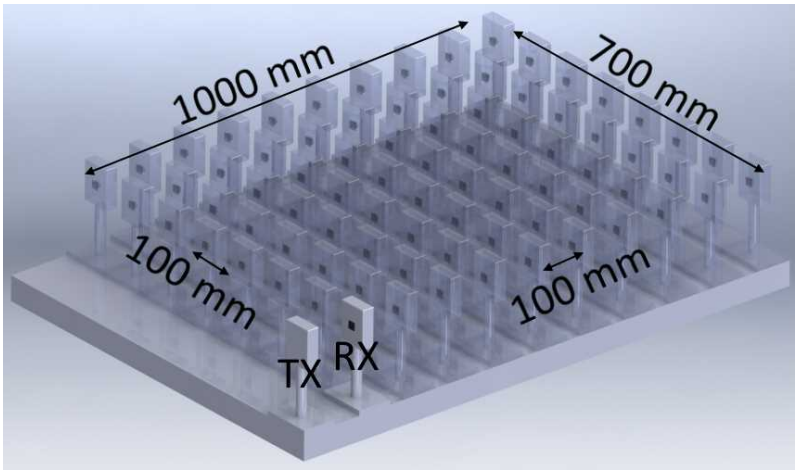

Figure 5.4: Optical bench used for the measurement campaign [67].

The LED is modulated via a sine-like signal with center frequency of 5

Table 5.1: Parameter legend

Parameter	Description
E	irradiance at the photodetector
P_i	incident optical power
S	photodetector sensible area
i_g	photodetector generated current
$R(\lambda)$	photodetector responsivity
V_t	transimpedance output voltage
r_t	transimpedance feedback resistance
V_o	amplifier output voltage
G_a	total amplifier gain

kHz (generated by a signal generator) spanning a range of amplitude from 2.3 to 4 V so that the source varies its emitting light power from 0 to 120 mW. For each position of the photodiode a portion of the received signal after the amplifying circuit is recorded with a digital oscilloscope. The amplitude of this signal is proportional to the irradiance at the detector since:

$$E = \frac{P_i}{S} = \frac{i_g}{S \cdot R(\lambda)} = \frac{V_t}{r_t}\frac{1}{SR(\lambda)} = \frac{V_o}{G_a}\frac{1}{r_t}\frac{1}{SR(\lambda)} \tag{5.1}$$

with parameter legend listed in Tab. 5.1.
Since the radiation propagation can be assumed symmetric with respect to XZ plane, the obtained irradiance pattern is depicted in Fig. 5.5. In the following the experimental data are analysed by introducing four physical propagation models that take into account different types of optical characteristics.

5.3.2 Experimental results

In order to find the mathematical model that best fits the experimental data, the following models are considered:

- Point source with spherical propagation.

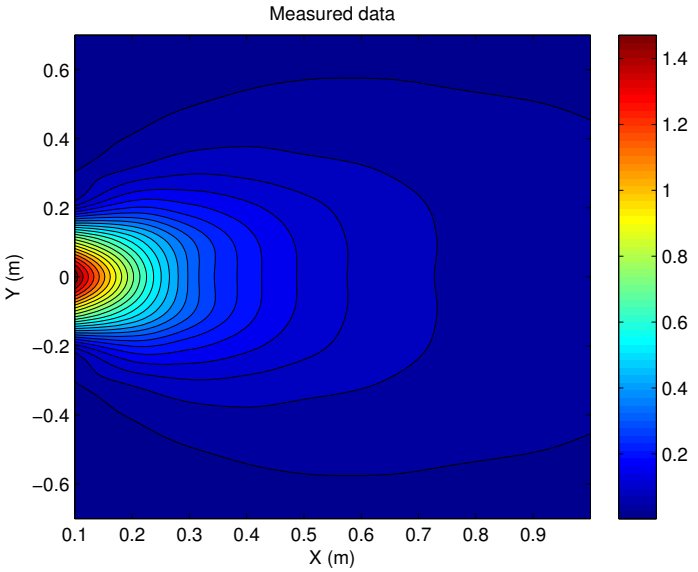

Figure 5.5: Irradiance as a function of detector position. The legend is expressed in Volts (V).

- Point source with Lambertian propagation.
- Point source with spherical propagation and reflection.
- Point source with Lambertian propagation and reflection.

Point source and constant spherical intensity model

First, let us define the receiver solid angle $d\Omega$ as

$$d\Omega = \frac{dS\cos\alpha}{r^2} \tag{5.2}$$

where dS is the photo-receiver surface, α is the angle between the x-axis and the line connecting the LED to the receiver, and r is the distance between the LED and the receiver. Using (5.2) we can obtain the radiation flux Φ:

$$d\Phi = I(\alpha)d\Omega = I(\alpha)\frac{dS\cos\alpha}{r^2} \tag{5.3}$$

where $I(\alpha)$ is the luminous intensity of the LED. Now, let us suppose that the source is point and the intensity is constant over the surface of a semi-sphere $I(\alpha) = I_0$. Then, the irradiance is

$$E = \frac{d\Phi}{dS} = \frac{I(\alpha)\cos\alpha}{r^2} = \frac{I_0\cos\alpha}{r^2}. \tag{5.4}$$

The irradiance E of (5.4) can be drawn as a function of the distance. Fig. 5.6a shows data results from the point-source-constant-spherical-intensity propagation model, while Fig. 5.6c shows the percentage error between the experimental data and the data derived by (5.4).
The error appears to be high and spread around. The average error is above 40%. Fig. 5.6b shows the quantity $E \cdot r^2$ for the experimental data (red line) and the data from (5.4). This first simple model does not fit the experimental data at all.

Point source and Lambertian intensity model

The second model now is assumed. The LED is still a point source, but a Lambertian model is considered for the irradiance. Then E is then given by

$$E = \frac{I_0(\cos\alpha)^2}{r^2}. \tag{5.5}$$

The obtained irradiance is reported in Fig. 5.7a while the quantity $E \cdot r^2$ for the experimental data (red line) and the data from (5.5) is reported in Fig. 5.7b.

Fig. 5.7c shows the percentage error between the experimental data and the Lambertian propagation model. Although the Lambertian model provides a better fit than the spherical model, the fitting is still not accurate.

Point source and constant spherical intensity model with reflection

The above mentioned models do not take into account reflections and it is quite evident that they do not correctly reproduce the experimental results. In fact, the average error is at least above 30%. In order to improve this result the surface reflection needs to be taken into account. In this particular experiment the optical bench is made of stainless steel so a specular reflection is assumed[1]. Let us consider a point source and a constant spherical intensity.

[1] Other surface materials are studied in Chapter 6.

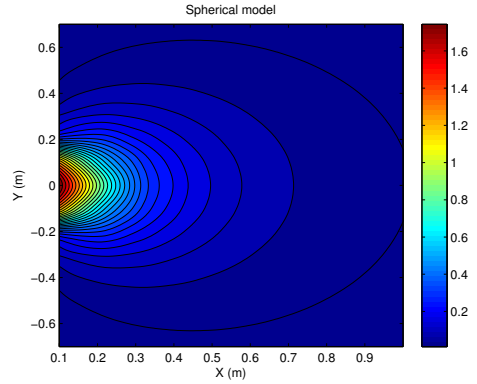

(a)

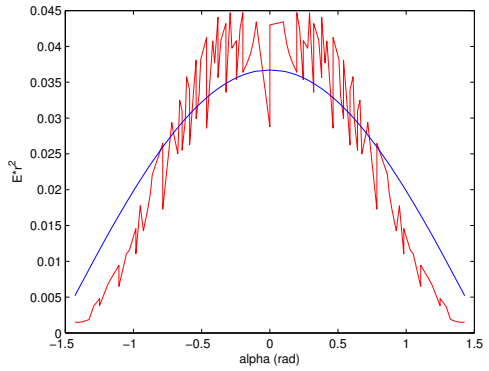

(b)

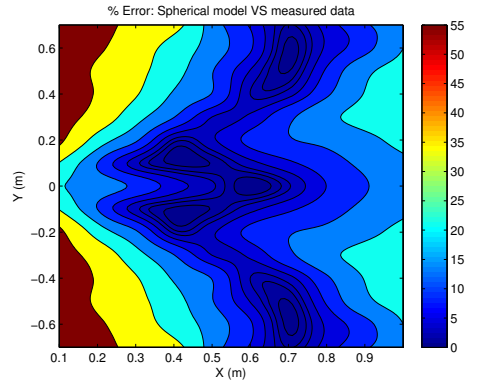

(c)

Figure 5.6: Spherical intensity propagation model: (a) data results from the propagation model (in Volt, V); (b) experimental data (red line) and propagation model (blue line); error (%) between the propagation model and the experimental data.

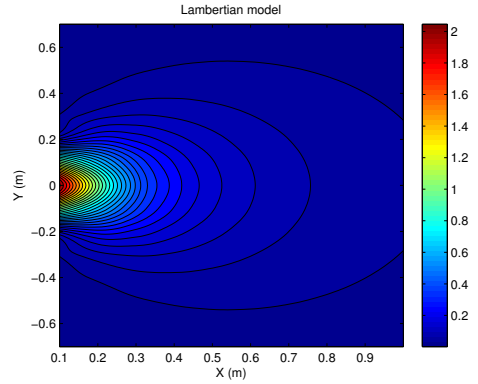

(a)

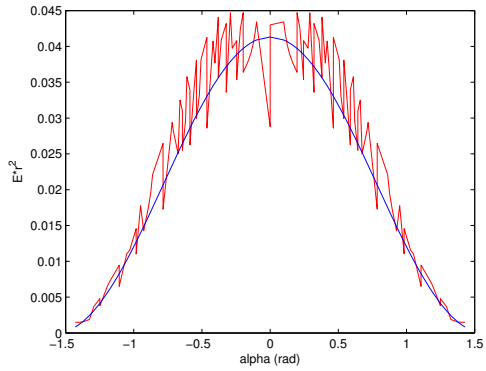

(b)

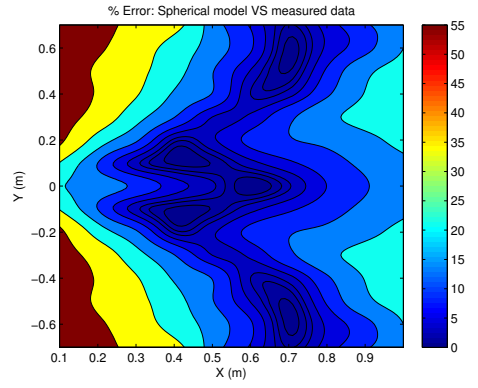

(c)

Figure 5.7: Lambertian propagation model: (a) data results from the propagation model (in Volt, V); (b) experimental data (red line) and propagation model (blue line); error (%) between the propagation model and the experimental data.

The irradiance, in this case, is

$$E = \underbrace{\frac{I_0 \cos\alpha}{r^2}}_{\text{Direct path}} + \rho \underbrace{\frac{I_0 \cos\alpha \cos\beta}{(h_{tx}+h_{rx})^2 + r^2}}_{\text{Reflected path}} \tag{5.6}$$

where $\rho \in [0,1]$ is the reflectivity of the bench surface and β is the angle of incidence of the radiation on the bench (see Fig. 5.8). It can be geometrically obtained from

$$\sin\beta = \sqrt{\frac{r^2}{(h_{tx}+h_{rx})^2 + r^2}} \tag{5.7}$$

with h_{tx} and h_{rx} being the height of the LED and the detector with respect to the optical bench surface (Fig. 5.8).

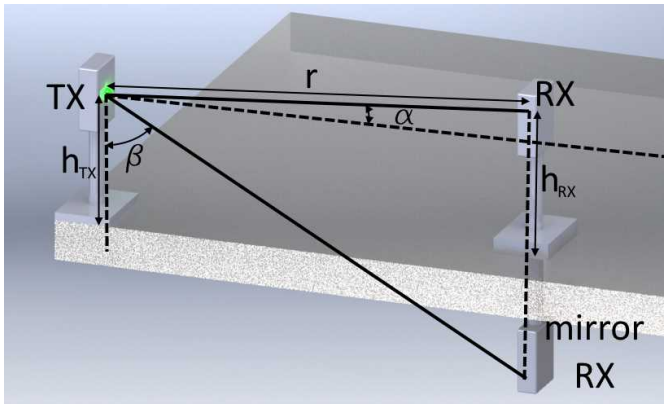

Figure 5.8: Angle and height parameters between source (LED) and receiver (photodiode) [67].

The obtained irradiance is reported in Fig. 5.9a whereas the quantity $E{\cdot}r^2$ for the experimental data (red line) and the data from (5.6) is reported in Fig. 5.9b. Even if by considering the reflection effect the error, shown in Fig. 5.9c, decreases and the model fits better the experimental data, the average error is around 20% and another model should be considered.

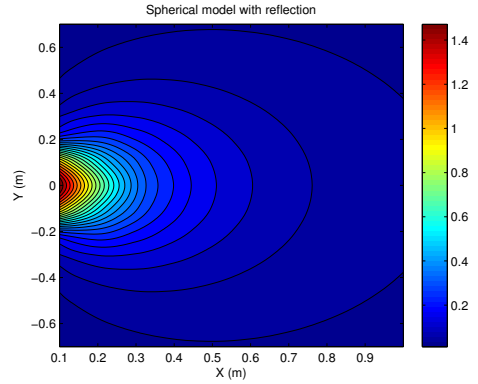

(a)

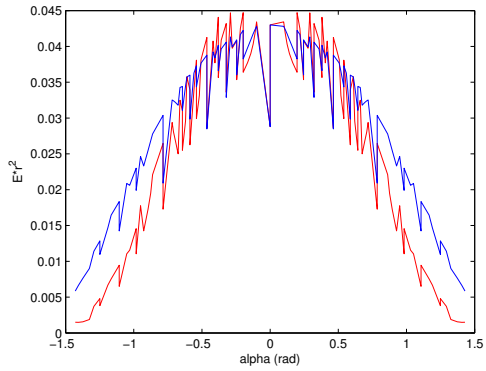

(b)

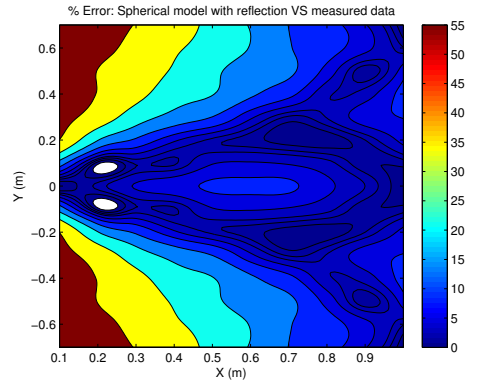

(c)

Figure 5.9: Spherical propagation model with reflection: (a) data results from the propagation model (in Volt, V); (b) experimental data (red line) and propagation model (blue line); error (%) between the propagation model and the experimental data.

Point source and Lambertian intensity model with reflection

The last model taken into account is a Lambertian model with reflection. With the same assumption made in Sec. 5.3.2,(5.5) can be modified as follows:

$$E = \frac{I_0(\cos\alpha)^2}{r^2}\left[1 + \rho(\sin\beta)^4\right] \tag{5.8}$$

where ρ is the bench surface reflectivity and β is the angle of incidence of the radiation on the bench. The reflection coefficient ρ can be used as a fit parameter to obtain a better agreement. As can be seen from Fig. 5.10c in this case the percentage error is almost everywhere below 10% except the points with large Y values. However, the measured irradiance for these points is extremely low, making them the least significant.

Fig. 5.10b shows the quantity $E \cdot r^2$ for the experimental data (red line) and the data from model (5.8), whereas the relative percentage error is reported in Fig. 5.10c. It is evident from Fig. 5.10 that the Lambertian model with reflection (5.8) fits well the experimental data.

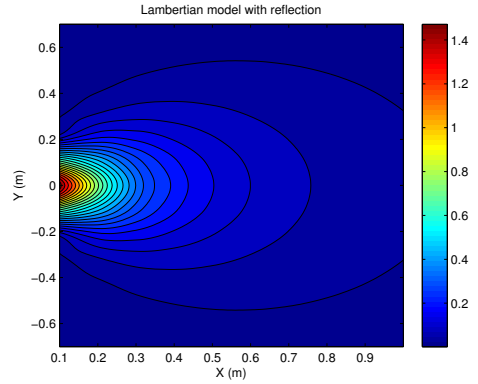

(a)

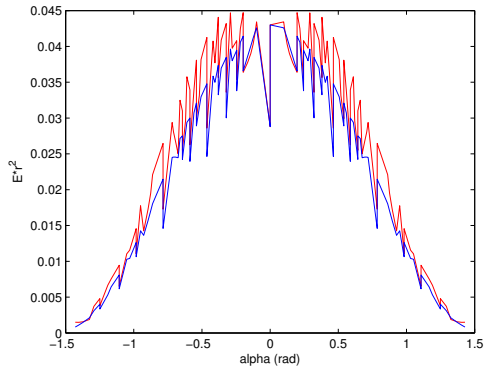

(b)

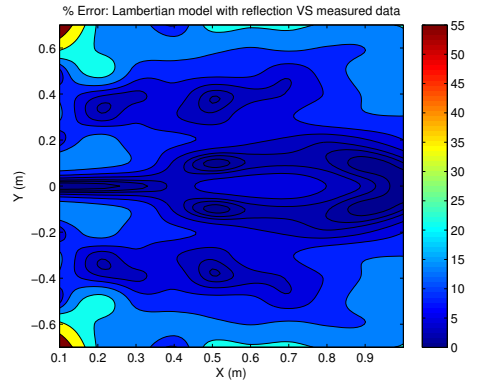

(c)

Figure 5.10: Lambertian propagation model with reflection: (a) data results from the propagation model (in Volt, V); (b) experimental data (red line) and propagation model (blue line); error (%) between the propagation model and the experimental data.

5.4 IEEE 802.15.7 complaint VLC transceiver

Here a first implementation of an IEEE 802.15.7 PHY-I complaint VLC transceiver is presented. In particular a small and simple VLC system is described. Both transmitter (TX) and receiver (RX) are designed and implemented from scratch using low cost electronic components. The physical layer follows the standard presented in Sec. 2.2 and, specifically, the "type I" is deployed, since it is meant for outdoor communication systems.

5.4.1 Hardware and Software

In the following a short description of the hardware and software suite used for designing the system is given.

Ettus USRP boards

Universal Software Radio Peripheral (USRP) is a range of SDR designed and sold by Ettus Research (now part of National Instruments) [9]. Usually implied for RF systems, the USRP family are designed for accessibility and many of the products are open source hardware (i.e. board schematics are freely downloadable). USRPs are commonly used with the GNU Radio software suite to create flexible SDR systems. In this thesis, SDRs are used only in their baseband stage since the information has to be transmitted through a visible light channel and not via an RF link.

Figure 5.11: Ettus Research USRP1 [9].

GNU Radio

GNU Radio is a free software development toolkit [5] that provides signal processing blocks for implementing SDRs and signal processing systems. It can be used with external hardware or without any equipment in a simulation-like environment. The GNU Radio software provides framework and tools to build and run software radio or general signal-processing applications. The GNU Radio applications themselves are generally known as "flowgraphs" (i.e. a high level programming model), which are a series of signal processing blocks connected together describing a data flow. As with all software-defined radio systems, reconfigurability is a key feature. Instead of using different transceivers designed for specific but disparate purposes, a single, general-purpose, radio can be used as the front-end, and the signal-processing software handles the processing to specific application.

5.4.2 System design

The VLC system is composed by a TX and an RX. Both terminals can be divided in three main functional blocks:

1. the electrical implementation of a transceiver (on a breadboard);
2. two Software Defined Radio (SDR) boards for interfacing the electrical part (ADAC stages) and handling the lowest ISO/OSI communication levels (data flows from and towards the higher levels);
3. two GNU Radio flowgraphs which implement the IEEE 802.15.7 protocol (PHY-I type level), control the USRP (Universal Software Radio Peripheral) boards and handle the higher ISO/OSI level towards the user. They also provide a HDI (Human Device Interface) with an user friendly interface.

As Fig. 5.12 shows two independent USRPs are used. Both terminals are controlled by the user exploiting a proper GNU Radio flowgraph. In here both the PHY layer and the user upper layers are implemented.

Transceiver electrical implementation

As mentioned before, both TX and RX are designed from scratch using low-cost electronics and simple configuration schemes. Fig. 5.13 and Fig. 5.14

show the electrical schematics for the transmitter and the receiver respectively. By referring to Fig. 5.13, a typical bias-T scheme (see Sec. 2.1) is implemented for polarizing the transistor in a liner region and allowing the signal coming from USRP's DAC modulate the current that passes through the LED. In this way the light intensity is modulated as the information bit arrives from the DAC. Figure 5.14 shows the front-end receiver. It consists of a high-pass filter and of a two-stage amplifier. This kind of amplifier is necessary as the output voltage coming from the phototransistor (PT) has to be adapted to the input range allowed by the USRP's ADC. Two diodes, placed between the first and the second, are used for clipping the signal, allowing the second stage amplifier to work always with the same values. Table 5.2 lists the main features of the IEEE 802.15.7 PHY-I complaint VLC transceiver.

IEEE 802.15.7 PHY-I level implementation

As referred in Sec. 2.2.2, IEEE 802.15.7 PHY-I is designed for outdoor usage. Here this type of standard's physical layer is implemented using GNU Radio. In fact, the aim of this part of the investigation is to design and implement a transceiver for vehicular VLC. In Fig. 5.15 the flowgraph of a complete IEEE 802.15.7 PHY-I transceiver chain is presented.

The transmitter part consists in (i) a HDLC[2] (High-Level Data Link Control) framer which builds a proper frame containing data and synchronization information; (ii) an OOK modulation with Manchester coding, and (iii) a raised-cosine filter for interpolating the signal, shaping the electrical pulse. Since a dispersive channel is supposed, this method (a pulse shaping filter similar to those used in RF wireless communications) helps minimizing the effect of signal distortion, i.e. the Inter-Symbol Interference (ISI) and control the BER. Moreover with this filter a synchronization block can be used at the receiver. More in depth, the receiver part is essentially composed by (i) an Automatic Gain Control (AGC), (ii) a synchronization and decimating block which recovers the timing from the frame header, (iii) an OOK demodulator that takes into account the Manchester coding at TX, and (iv) a HDLC de-framer which extracts the information. "USRP sink" and "USRP source" blocks are used for sending/receiving data flows to/from USRPs.

[2]HDLC is a bit-oriented code-transparent synchronous data link layer protocol developed by the International Organization for Standardization (ISO).

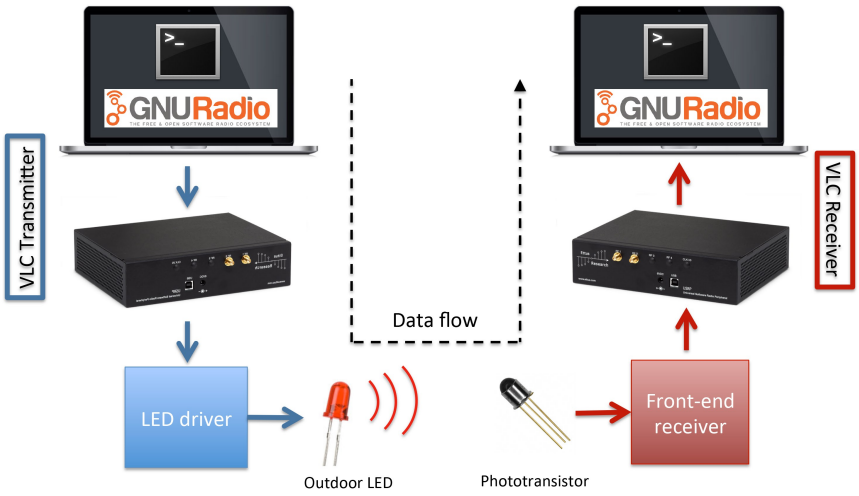

Figure 5.12: VLC transceiver block scheme.

Table 5.2: VLC transceiver features.

Parameter	Value
Terminals	2 USRPs
LED	CREE C503B
LED luminous flux	5000 mcd
LED FOV	46°
LED spectral wavelength	624 nm
PT	Vishay BPW77NA
PT FOV	20°
PT spectral range	450 - 1080 nm
PT cut-off frequency	110 kHz
Sampling	12 bits @200 kHz

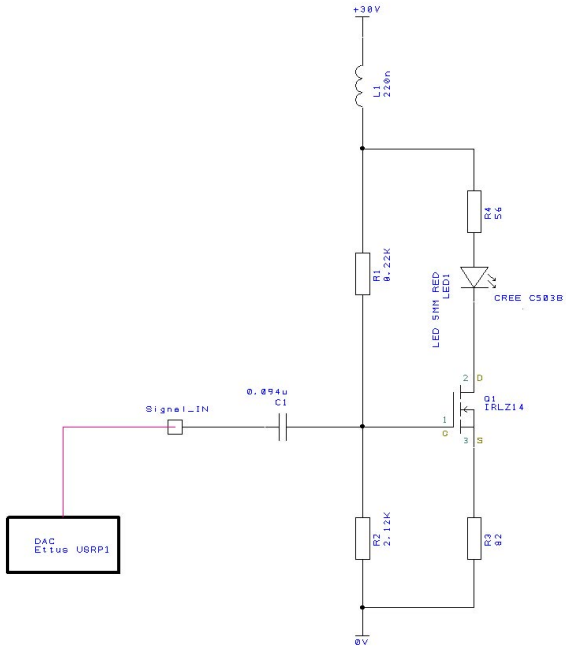

Figure 5.13: VLC transmitter electrical schematic.

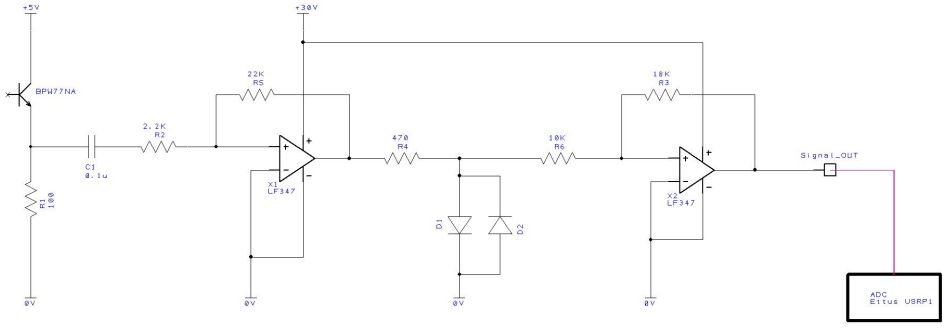

Figure 5.14: VLC receiver electrical schematic.

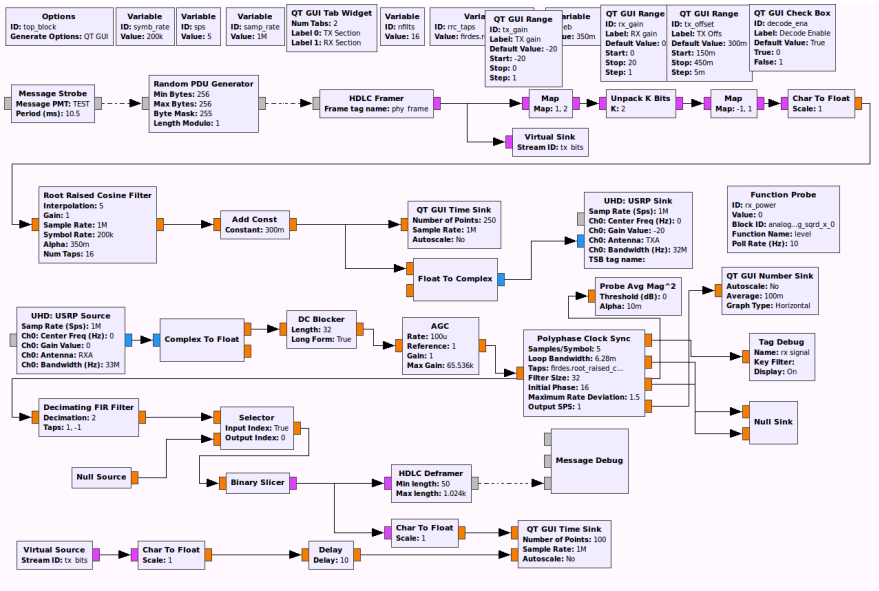

Figure 5.15: GNU Radio flowgraph - IEEE 802.15.7 PHY-I.

Experimental preliminary tests

Figure 5.16a shows the LED driver and the front-end receiver presented in schematics of Fig.s 5.13 and 5.14, respectively. A breadboard electrical implementation is deployed using low-cost components. The full laboratory bench is shown in Fig. 5.16b. Here two different computers connected via USB with two USRPs are used. One platform for each terminal is deployed. Using the GNU Radio flowgraphs of Fig. 5.17 and 5.18[3], for TX and RX respectively, an UDP connection is established. Both an "iperf" bandwidth test at 100 kbps and an audio stream (an 96kbps stereo mp3 file, at 44100Hz, with Variable Bit Rate) transmission are successfully performed. The system is able to work also in the presence of direct ambient light, within a distance of 30 cm between the two terminals. Larger distances could be achieved by, both, using a much powerful light source or by employing a more sensitive receiver.

[3]Basically, the complete transceiver chain flowgraph of Fig. 5.15 has been divided in two fundamental parts, one implementing the TX side and one the RX side.

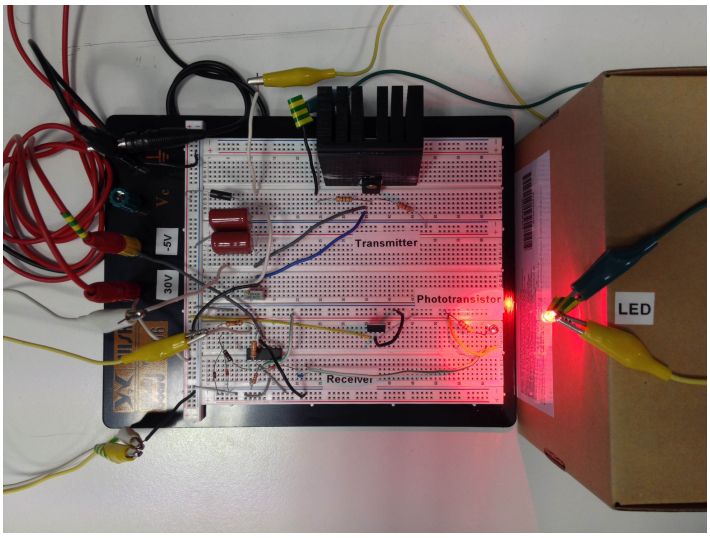

(a) Transceiver electrical implementation.

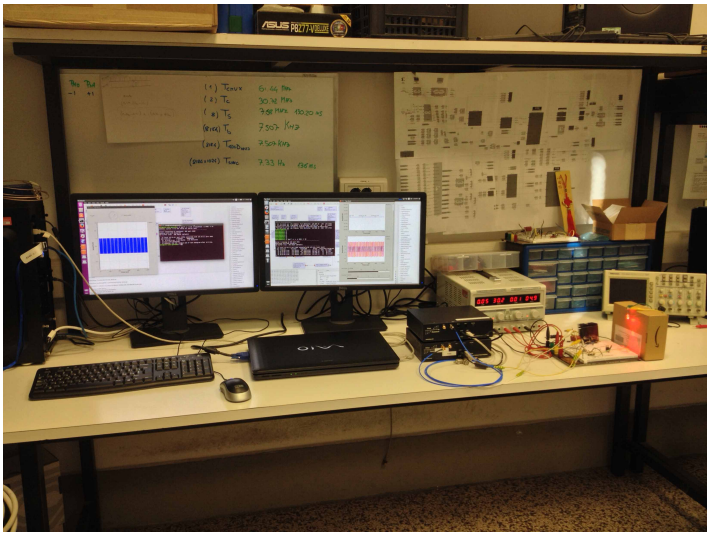

(b) Testbench overview.

Figure 5.16: Preliminary transceiver test.

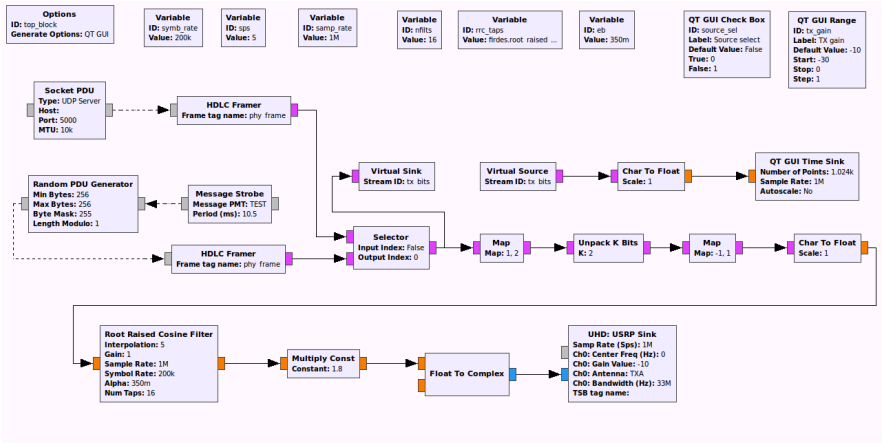

Figure 5.17: GNU Radio flowgraph - VLC Transmitter.

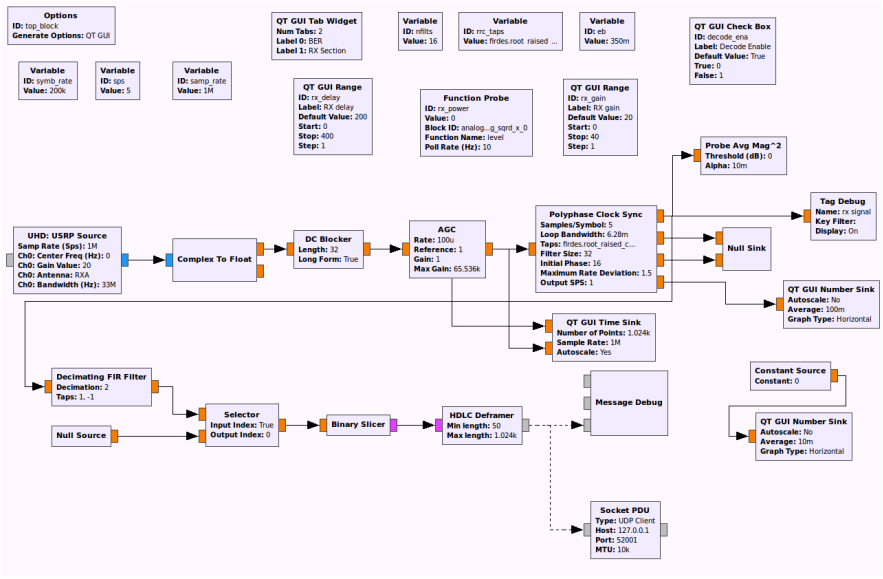

Figure 5.18: GNU Radio flowgraph - VLC Receiver.

Chapter 6

Filtering Out Reflections in Low-cost LED-based Positioning System

This chapter proposes a new multipath detection technique for positioning with light that does not require the knowledge of the channel impulse response, and that it is suited to be implemented in low-cost positioning receivers that use a single photodiode. To develop the technique, (i) the statistical properties of Non-Line-of- Sight (NLOS) components are analyzed, (ii) an automated testbed to study the reflections of different types of surfaces and materials is developed, and (iii) an algorithm to remove the NLOS components affecting the positioning is designed. The experimental evaluation shows that in complex environments the proposed methodology can reduce the localization error using LEDs by 93%.

6.1 Introduction and motivation

As described in Sec. 1.1, artificial lighting is everywhere, from the light bulbs on our ceilings to car headlights. It is expected that before 2020, there will be 6-7 billion LED lights worldwide [6]. This trend makes VLC an attracting technology for data, and more recently, to locate objects and people using

LED-based Positioning Systems (LPS). LPS is gaining a lot of attention from industry and the scientific community due to their high accuracy.

Broadly speaking, LPS can be divided into two categories depending on the type of optical receiver they use: photodiode (PD) or image sensor (camera) [52, 55, 89]. PDs provide higher throughput and energy-efficiency than cameras, and thus, are a better choice for wearable devices (low energy) and vehicular networks (high throughput). Image sensors are popular due to their widespread availability in smartphones, but they have a reduced data rate (only kb/s rather than Mb/s or more [42]) and a higher energy cost (in the order of 300 mW rather than a few mW [56]).

While the area of LPS for smartphones is relative mature with products already in the market [8], this is not the case for LPS in wearable devices and vehicular networks in real environments. Compared to cameras, the main constraint of PDs is their sensitivity to interference caused by optical reflections: all incoming optical rays sum up at the PD because it operates as a single pixel [38]. Image sensors can instead solve optical interference by exploiting multiple pixels [72]. Therefore, LPS with PD receivers are affected by location errors in real deployments [38].

Discerning the direct Line-of-Sight (LOS) path for positioning using a PD receiver is not a trivial issue. Estimating the channel response to infer the direct and reflected Non-Line-of-Sight (NLOS) paths requires a powerful analogue-to-digital converter (ADC) and high processing capabilities on the receiver side, which may not be available or desired [64]. Reflected paths have been ignored in several recent experimental papers [36, 55, 87]. Instead, the characterization of reflected paths has been done prevalently using simulations, and their detection/discrimination (seen as multiple sources) has been done with cameras and image processing techniques [29, 32].

6.2 Contribution

Within this context, the main contribution of this thesis part is the ability to experimentally discern and filter reflected paths using a single PD. The key idea is to trade-off the need for in-depth knowledge of the channel with the instantaneous channel impulse response, with a less complex yet practical approach based on time series of the Received Signal Strength (RSS) collected with a low-cost PD. This trade-off is possible in the considered scenarios (vehicular and wearable networks) because:

1. nodes are mobile, and thus, changes in reflection occur over a short period of time;

2. the reflections from materials have unique statistical properties that can be exploited to filter out NLOS components;

3. our scenarios can accept some marginal delay, which allows us to work with short time series.

To wrap up, the main contributions of this work are:

- Sec. 6.5: The first testbed that allows to make controllable and realistic down-scaled characterization of visible light multipath in low-cost receivers, as caused by various types of surfaces.

- Sec. 6.6.5: A statistical method to identify and discriminate Non-Line Of Sight (NLOS) components with limited sampling rate of the receiver.

- Sec. 6.7.3: A decision tree algorithm that can run in low-cost receivers and it uses only two observables, yet it can differentiate between different types of reflections.

- Sec. 6.7.4: We remove NLOS components and the experimental evaluation shows that our method can improve the accuracy of LPS up to 93%.

6.3 State of the art

The majority of the related works about visible light reflections considers indoor scenarios. Mainly studied through simulations [15], most of works rely on the ray-tracing algorithm in which different reflection patterns (e.g. Lambert-Phong) are exploited [32]. Optical and illumination design software like Zemax [10] are employed for modeling complex indoor scenarios. Reflective material and node mobility lead to significant RSS variation introducing shadowing and performance degradation (higher Bit-Error-Rate) depending on the scenario [33]. Generally speaking, reflections bring interferences, limiting data rate with the need of an equalizer for compensating the undesired effect [64] and [37].

Reflective material shape and relative height between TX and RX also lead to intensity variation [86]. Simpler NLOS analyses consider each reflection point on surfaces as a new LOS optical source [32] and, typically, no more than 3 reflection paths are considered since later paths do not bring significant contribution in terms of RSS variation [86]. Different types of material emit different kinds of reflection, and the pattern reflected by the surfaces has to be taken into account when reflections are modeled for indoor channels [26,58]. Closeness of the direct light path to reflective surfaces of course count in varying significantly the RSS, but many reflection paths cannot be taken into account since they are not intercepted by the receiver incidence angle [38]. [24, 25] have performed an efficient characterization of the NLOS components to model Channel Impulse Response. In some cases, taking advantage of indirect paths is also possible, exploiting the time difference between the LOS and the first reflection [41]. These solutions come at the cost of high computational resources, even if only up to 2nd order reflections are considered.

The NLOS component also affects LPS [61,65] as the positioning error increases linearly with the reflection coefficient of materials [85]. A multipath-related severe error (from a few cm to 1 m) has been reported when it is taken into account in LPS [38,39,77]. Proper countermeasures need to be adopted for avoiding the localization error. A LOS-NLOS identification algorithm exploiting different LED IDs for calculating the Signal-to-noise Interference Ratio have been investigated to reduce the impact of multipath [43]. Yet, this approach requires a sufficient number of LED luminaries, which may not be available. Image sensors are also often used for canceling the effect of reflections and get more reliable systems [72]. Image sensors have been often employed also for analyzing vehicular VLC channels and estimating how the path loss varies over time in real traffic scenarios [29, 30, 84]. However, they come with much higher energy consumption cost and lower data rate of communication. If simple scenarios are assumed, propagation and multipath models obtained for indoor have been used for outdoor modeling [60] even if more complex mobility scenarios need to be simulated with specific software [54, 75], with limited practical usage for low-cost systems. Realistic headlamp pattern models [60], car rotations [63] or vehicle vertical movements due to road surface irregularity [23], link asymmetry in mobility [78] and vehicles reflective surfaces [57] have been studied for deriving the effect signal variation and the performance of C2C (Car-to-Car) VLC systems.

6.4 Motivation

This section, first introduces the predictable channel attenuation model used by all previous practical works in LPS [36,52,55,87,89], and we show through experiments that reflections negatively affect LPS with PD receiver. Then it presents the basic intuition behind the proposed solution and the research challenges which need to be addressed.

6.4.1 Positioning with reflected light

The inverse-square law accurately characterizes the relation between distance and RSS in pure LOS scenarios. Here this finding is validated changing the distance between the Transmitter (TX) and a low-cost PD Receiver (RX), and collecting RSS measurements. The results in Fig. 6.1 show that there is a good match between theory and practice, with only a small deviation at short distance due to the saturation of the low-cost receiver. This good match has been the foundation behind all the uptake of LPS in the last few years. Yet, this monotonic curve becomes less predictable and more noisy if a fraction of the light does not reach the RX through the LOS link, but current experimental studies do not quantify this phenomena.

From theory, when light hits a surface, there are three possible outcomes. Light may be absorbed by the material, it may go through the surface or it may be reflected, creating the NLOS link. Materials often show some mix of these behaviors, with the proportion of light that goes to each component depending on the properties of the material, the wavelength of the light, and the angle of incidence. Reflections affect LPS working with a PD receiver because the primitive used by the majority of solutions for positioning is the super-imposition of received signal strength (RSS) from all components [89].

In order to quantify the impact of reflection, first, the ideal environment (considering only the LOS component) is considered, and subsequently, the presence of different materials reflecting light are included. Using the experimental setup presented in Sec. 6.5, the distance from a TX and a RX based on the power received is estimated. For the test, the TX and RX are placed at different distances, and at each distance, the range following the inverse-square law [89] is estimated (see Fig.6.1). As the aim is to study realistic mobile scenarios, here are considered different reflective indoor and outdoor materials.

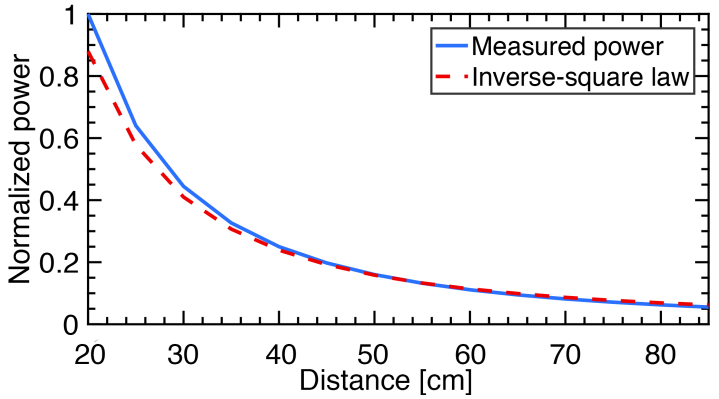

Figure 6.1: Comparison of inverse-square law with respect to RSS measurements using low-cost PD receivers in ideal LOS links. The study shows that there is a good match between theory and practice. Power normalized w.r.t. the maximum value.

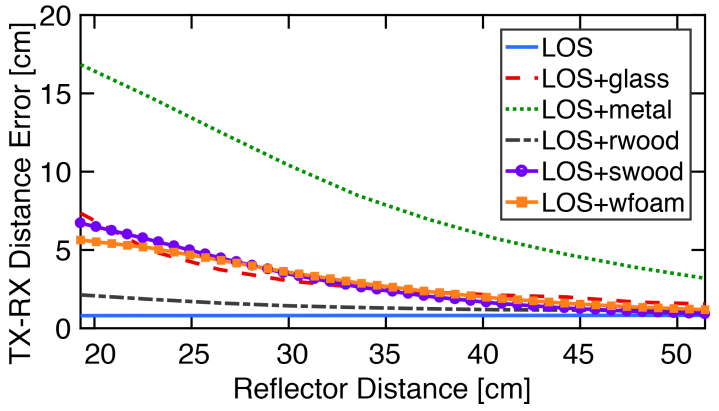

Figure 6.2: Experimental distance error. Reflections increase the error in the positioning system. The error depends on the type of material (glass = shiny glass, metal = grey satin metal, rwood = chipboard, swood = plywood, wfoam = foamcore).

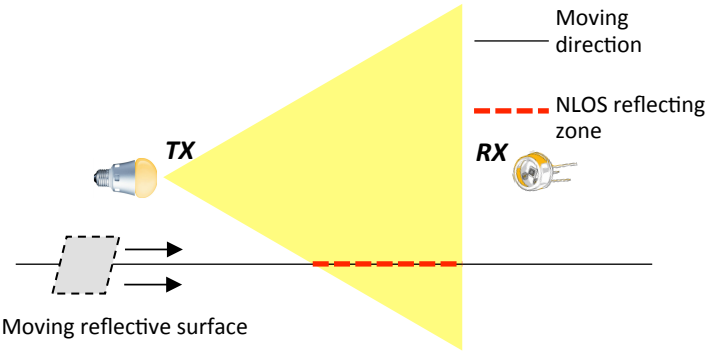

Figure 6.3: Schematic representation of reflections in the presence of mobility. The red dotted line depicts the reflecting zone.

Subsequently an evaluation of the distance error[1] with respect to the distance to the reflective material is performed using the algorithm proposed in [36]. The results are plotted in Fig. 6.2. From the plot it can observed that the smallest error is obtained when there is only a LOS component (no reflective material), as expected. In this case, the position accuracy is 0.55 cm. Depending on the reflective material, the relative error can be up to 4 times the minimum error, decreasing the accuracy of any localization system (up to 11.76 cm of error). Also it can be observed that the error is different for each material, since each material interacts in a different way with light.

6.4.2 Basic Intuition behind the proposed solution

The detection of NLOS components could be performed in systems with an expensive receiver with high gain-bandwidth product that sample quickly the channel impulse response [26]. This requires a very fast impulse generator at the transmitter and a very high sampling rate at the receiver. In low-end systems, these requirements are not feasible. Instead of looking at the instantaneous Channel Impulse Response (CIR), here it is exploited the fact that, in a dynamic environment, a reflector does not appear suddenly, but instead enters the illuminated area and the reflections are received by the PD at a certain speed (creating the NLOS component), c.f. red dotted

[1]Percent distance error means the positioning error w.r.t. the ground truth, that is equal and fixed to 70cm.

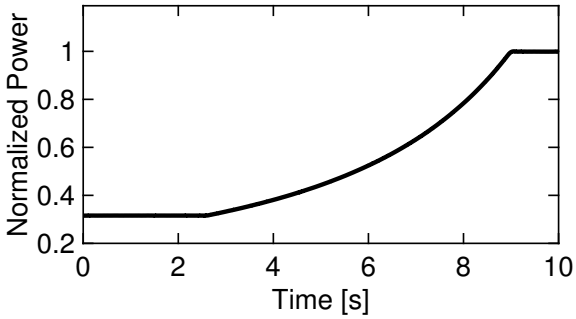

(a) Slow relative speed.

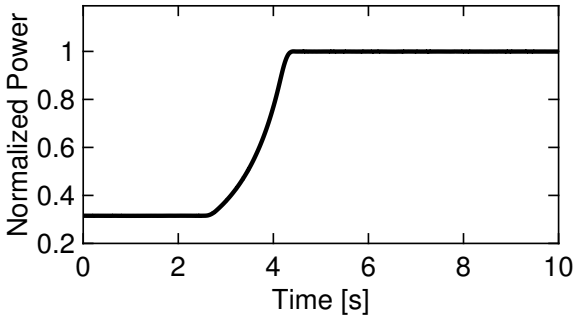

(b) Fast relative speed.

Figure 6.4: The RSS (shown as normalized power w.r.t. the maximum value) also changes when the TX and RX get closer to each other. Faster speeds create steeper slopes.

line in Fig. 6.3[2]. Over time, the receiver first observes an RSS variation due to the transition between the LOS and "LOS+NLOS" components, and subsequently, a transition between the "LOS+NLOS" and LOS components (when the reflective material is moving away).

[2]In this work a mobile reflector and static TX and RX are considered, but the same concept applies to other cases, such as mobile TX and RX and a static reflector; or mobile TX and RX and a mobile reflector at different speeds.

6.4.3 Challenges

This study addresses three main problems (P) in LPS:

P1. *Do not filter out valid RSS variations caused by relative changes in distance and rotation between TX and RX.* At first sight, eliminating reflections may look like a simple problem. Given that reflections only increase the light intensity, a naive solution would be to use a peak-removing algorithm to obtain the baseline RSS. Changes in RSS, however, are also caused by relative movements between the TX and RX, and these dynamics should not be filtered out since they are indispensable for an accurate position estimation [36]. As shown in Fig. 6.4, when the TX and RX get closer to each other, the RSS increases with the relative speed of the movement. The presented method relies on a simple PD to discern changes in RSS caused by legitimate movements and by undesired reflections.

P2. *Identify reflections caused by different types of materials.* There is no one-size-fits-all metric to detect reflections. Reflections have unique properties depending on the type of material and how the light is reflected on the surface. Here is proposed a robust yet-simple mechanism to identify reflections from a wide variety of materials without having the luxury of performing the CIR.

P3. *Controlled experimental environment.* Arguably, one of the main roadblocks in the community to study the effect of reflections in LPS is the difficulty of performing controlled and replicable experiments. From the author's knowledge, there is no such infrastructure in the community. Due to this reason, most studies focus only on theory and simulations [38,39,41,43, 61,65,77,85]. A key contribution of this work is the design of a novel mobile testbed to analyze and improve the performance of LPS.

6.5 Testbed

6.5.1 Description

Moving from the realm of theory and simulations into empirical evaluations requires a testbed. The first challenge was to solve **P3**. A testbed with modules capable of providing light-based positioning and mobility is required. To tackle the positioning requirement, the OpenVLC boards are used for LPS algorithm [36]. To tackle the mobility requirement, these boards are mounted onto a structure that was originally designed for medium-scale 3D printing:

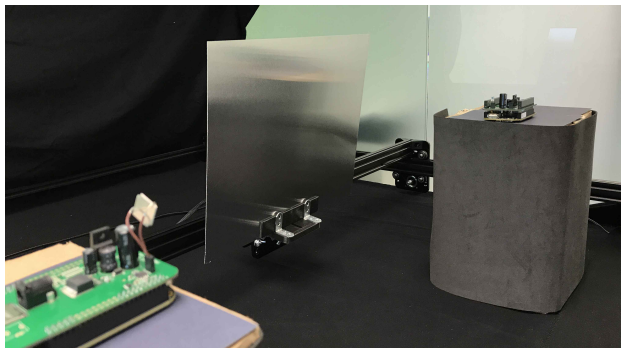

Figure 6.5: Testbed.

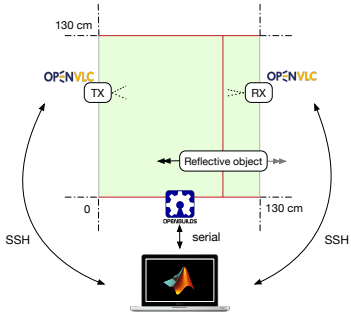

(a) System schematic with material moving in the x-axis.

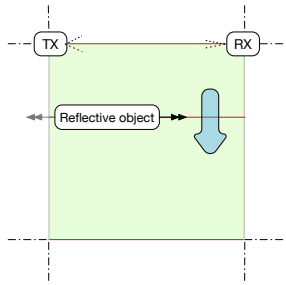

(b) System schematic with material moving in the y-axis.

Figure 6.6: Testbed: the material moves in both the x and y-axis.

the OpenBuilds ACRO movement structure [3] (see Fig. 6.5). These two systems are then bundled together (mechanically, electrically and with software) to provide a precisely controlled environment. The testbed deployed here can reproduce fully customizable down-scaled mobile scenarios and automatizes the collection of raw data. Without loss of generality, the reflecting materials are moved and the TX and RX are kept fixed (as the movement can be considered relative). The reflective surface is fixed on top of the mobile unit of the system (see Fig. 6.6a), and it can move at a maximum speed of $1.5km/h$ and a maximum acceleration of $2m/sec^2$ per axis. Table 6.1 reports the features of our testbed.

Table 6.1: Testbed features.

Parameter	Value
Nodes	2 OpenVLC units
LED luminous flux	956 lm
LED FOV	110°
LED spectral range	380-780 nm
PD area	7.02 mm^2
PD FOV	120°
PD spectral range	400-1100 nm
PD spectral sensitivity	80 nA/lx
Sampling	12 bits @200 kHz
Movement grid	130 cm x 130 cm

All the experiments use the following setup. The TX, which emits a fixed light intensity, and the RX are placed at a distance of 70 cm. The RX acquires a trace of 7.5 seconds (i.e. 1.5 million samples) for each movement[3]. The same measurement is repeated 30 times in order to have statistical relevance. To consider various distances between the LOS and the reflecting materials (blue arrow in Fig. 6.6b), the test starts from a lateral distance of 20 cm, and then moves the reflective surface down in steps of 5 cm up to a distance of 65 cm (10 different distances). 300 traces are collected for each material, plus another 300 for the "pure LOS" condition.

6.5.2 Materials employed

As realistic mobile scenarios have to be studied, some typical, indoor and outdoor, materials are considered in the experimentation. In particular:

1. Glass (sample of acrylic shiny glass, $420x297mm$, Fig. 6.7a);
2. Metal (sample of grey satin metal sheet, $320x320mm$, Fig. 6.7b);
3. Foam (sample of foam core, $320x320mm$, Fig. 6.7c);
4. Wood (sample of plywood $320x320mm$, Fig. 6.7d);
5. Chipboard (sample of $320x320mm$, Fig. 6.7e);

[3]Each movement consists of a back-and-forth object shift.

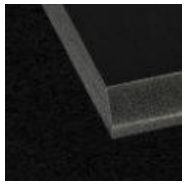

(a) Acrylic glass.

(b) Satin metal.

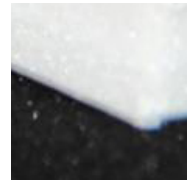

(c) Foam core.

(d) Plywood.

(e) Chipboard.

Figure 6.7: Sample materials used in the experimentation.

are employed. Selected samples have different reflective properties and, in particular, they are supposed to have progressively less specular-like reflection (from glass to chipboard) or, vice versa, more diffuse-like reflection (from chipboard to glass).

6.5.3 Validation tests

In order to validate the reliability and to characterize our testbed, here are performed a set of experiments. In particular, the environment and derived the acquisition noise are experimentally analysed.

Environmental and system noise analysis

For ensuring an external-interference free testbed, the movement grid is covered with a black cotton blanket[4]. Figure 6.8 shows the reliability of the test in terms of avoiding external interferences (e.g. a Continuous Wavelet Transform (CWT) is presented). More in detail, by comparing Fig. 6.8a and Fig. 6.8b, it can be noted that all the strongest frequency components (both at 100 Hz and 40 kHz[5]) are removed just by placing the receiver inside the

[4]This kind of blanket is usually employed as a background in studio photography for absorbing unwanted scattered light.

[5]By referring to Fig.6.8a, both these components (and their harmonics) are due to the artificial illumination (neon) of the laboratory. 100 Hz is the fundamental frequency of

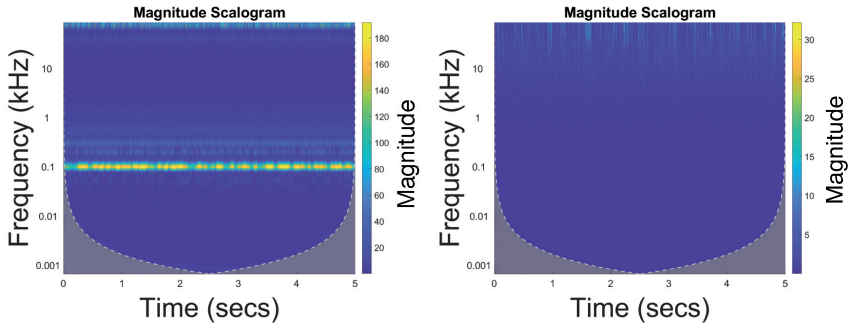

(a) Receiver placed outside the box. (b) Receiver placed inside the box.

Figure 6.8: External interference analysis made with CWT.

testbed "box".

LOS characteristics

Here the statistical results for the pure LOS test are shown (see Fig. 6.9). In particular, mean value, median, standard deviation and variance are presented. As it can be seen from plots, experiments can be repeated in the testbed with a good precision[6], since acquired values show a low uncertainty (e.g. the mean value uncertainty is 2,024 while the standard deviation uncertainty is 0,064).

6.6 Identifying reflections

As stated in Section 6.4, removing the effects of reflections in LPS implies identifying those reflections (**P2**) and discerning valid RSS changes (**P1**). In this section, the identification problem **P2** for a series of RSS measurements is tackled. Instead, the differentiation problem is tackled in the next section.

these type of illumination, while 40 kHz is due to the switching power supplies inside each neon.

[6]Accuracy calculation was not possible since any measured reference value of light intensity was given.

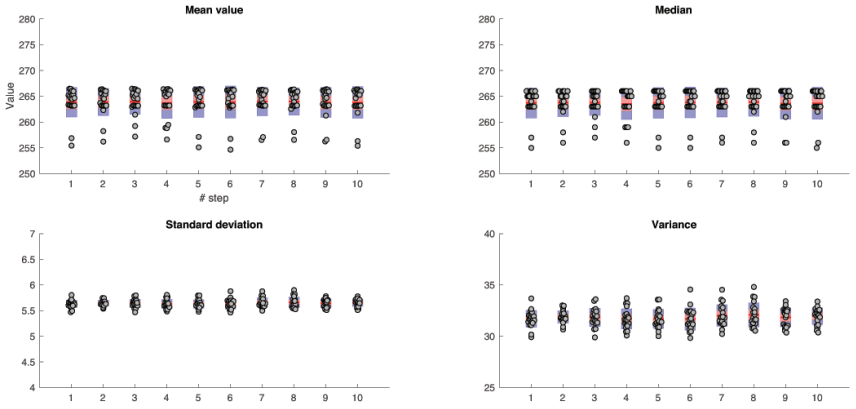

Figure 6.9: Pure LOS statistical results.

6.6.1 Understanding reflection 'peaks'

Reflections cause peaks in light intensity, but these peaks can take widely different shapes depending on the properties of the reflecting material. The first task is to define a minimal set of features to identify all such peaks. When light impinges upon a material, all reflected components are summed-up at the receiver. The final received intensity depends on two key properties. First, the reflection coefficient, the more reflective the material is (e.g. a mirror), the higher the light intensity reflected. Second, the material's smoothness, a very diffuse material (e.g. white paper) has a wide contribution because it reflects light in all directions, c.f. Fig. 6.10a. This type of materials lead to short but wide reflection peaks, c.f. Fig. 6.11a. A specular material on the other hand (e.g. a smooth metallic plate) will only reflect light near the Snell angle (Fig. 6.10b). These specular materials lead to tall but narrow peaks, c.f. Fig. 6.11b. Furthermore, the shape of the peaks is also affected by the size of the reflective material (bigger materials lead to wider peaks), and by their relative speed (slower speeds lead to wider peaks). The number of materials, and their various sizes and speed, would lead to a large number of peak shapes. The identification approach should be material-, size- and speed-independent.

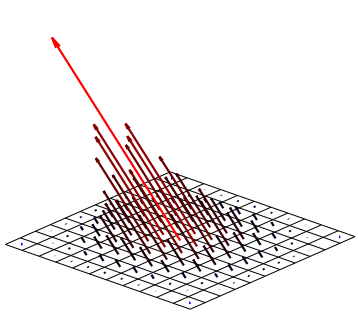

(a) Light rays on diffuse material.

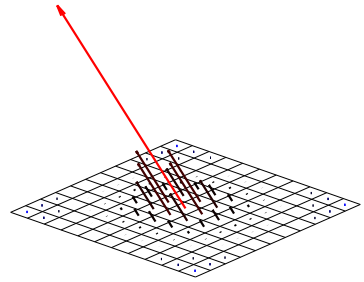

(b) Light rays on specular material.

Figure 6.10: Light reflection on diffuse and specular materials.

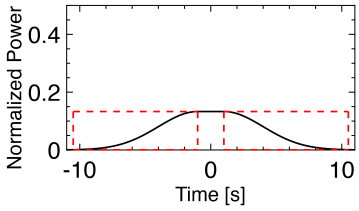

(a) Power received when a diffuse object moves into an illuminated area.

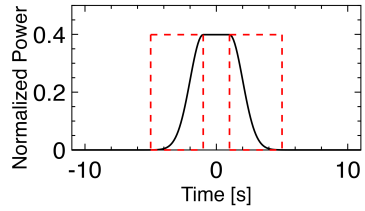

(b) Power received when a specular object moves into an illuminated area.

Figure 6.11: Power received over time at the receiver with diffuse and specular materials.

6.6.2 Making the approach size independent

The common trend in all reflection peaks is that the power received by the NLOS component increases when the reflective object enters the illuminated area, reaches a maximum when all the material is illuminated and starts decreasing when the material gets out of the illuminated area. The plateau of the peak is determined by the size of the reflective material. Thus, to make the system size-independent here it is proposed to focus solely on the intrinsic properties of the channel transitions, that is the upward and downward slopes, c.f. Fig. 6.11 red dotted squares. The mechanism to select these slopes from the trace is explained later in this section. For now, the focus is on analyzing the distribution of the light intensity.

Let us consider a "Pure LOS" scenario and four "LOS+NLOS" scenarios composed by materials with distinct reflective features (glass, metal, plywood and chipboard). Using the experimental setup introduced in Section 6.5, in Fig. 6.12a is depicted the raw trace and distribution for the "Pure LOS" condition. As expected, the distribution is a normal distribution with $\mu = 238$ and $\sigma = 2.91$. For the "LOS+NLOS" scenarios, there are some peaks that would lead to localization errors, c.f. Fig. 6.12c-6.12j. To highlight the behavior hidden underneath the environmental noise, a moving average filtering (white line) is shown. Except for the chipboard, which has a minimal effect due its low reflection coefficient and diffuse reflection, all the other materials have bimodal distributions. These bimodal distributions have different trends, but all distributions are clearly distinguishable from the "Pure LOS" case. As an example, glass produces a sharper reflection than metal or plywood. Here *sharp* means that the incoming signal at the receiver has fast slopes when the object enters the illuminated area. This property can be evaluated from the histogram since the received signal, when glass is considered, has two well separated groups of values (i.e. bimodal distributions, see Fig. 6.12d). Instead, signals related to metal or plywood interference have smoother transitions (Fig. 6.12e and Fig. 6.12h). Finally, chipboard is the less reflective object of this sets as the received signal and its histogram look very close to the "Pure LOS" condition. The important insights are that these bimodal distributions are i) a representation in the time domain of the channel impulse response, and ii) solely caused by the slopes, not by the plateau (which only adds samples to the main AWGN, Additive White Gaussian Noise, distribution), and thus the system is size-independent.

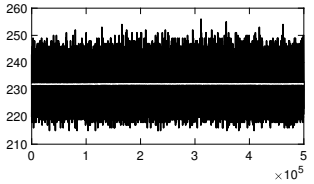

(a) Pure LOS - raw data.

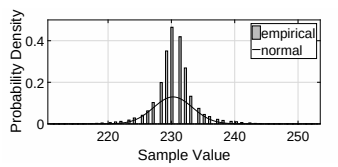

(b) Pure LOS - hist. and fitting.

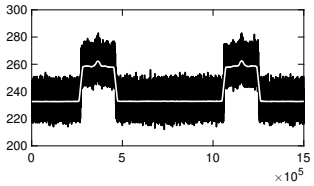

(c) Glass - raw data.

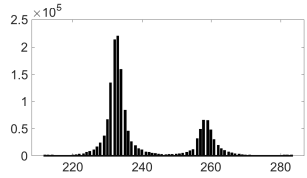

(d) Glass - histogram.

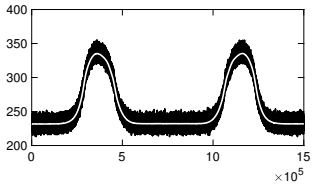

(e) Metal - raw data.

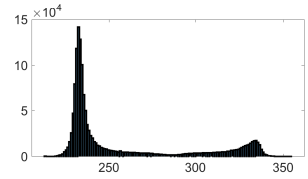

(f) Metal - histogram.

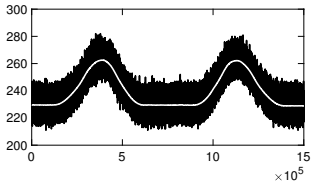

(g) Plywood - raw data.

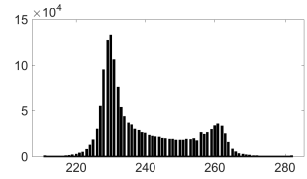

(h) Plywood - histogram.

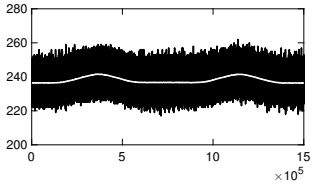

(i) Chipboard - raw data.

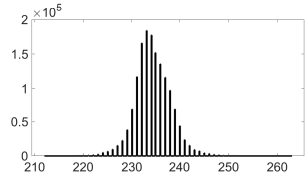

(j) Chipboard - histogram.

Figure 6.12: Typical raw signal for "LOS+NLOS" condition with sample materials. Left to right: raw data and smoothed signal (sample number on x-axis and sample value on y-axis), histogram (sample value on x-axis and number of occurrences on y-axis).

6.6.3 Statistical analysis

As said previously, the algorithm should try to exploit the peculiar characteristics of the variation in the received signal when light bounces on a given surface. With the constrain of using a given sequence of RSS samples collected with low-cost receivers, here it is proposed to look at the statistical moments up to the 4-th order as candidate observables to monitor the channel transitions of the NLOS component, and identify those material properties. Apart from the mean μ, and the standard deviation σ, then the skewness $skew$ (third order) and the kurtosis k (fourth order) are considered.

$$skew = E\left[\left(\frac{X-\mu}{\sigma}\right)^3\right], \tag{6.1}$$

where E is the expectation operator, Kurtosis is a measure of whether the data are heavy-tailed or light-tailed relative to a normal distribution. That is, data sets with high kurtosis tend to have heavy tails, or outliers. Vice versa, distributions with low kurtosis tend to have light tails, or lack of outliers. Whereas the kurtosis k is:

$$k = E\left[\left(\frac{X-\mu}{\sigma}\right)^4\right]. \tag{6.2}$$

The reference standard is a normal distribution, which has $k = 3$. The skewness gives the amount and direction of skew (departure from horizontal symmetry), and kurtosis gives how tall and sharp the central peak is, relative to a standard bell curve (i.e. normal distribution) [17]. Since only low-computation solutions are considered, in here Higher-Order Statistics (HOS) are not taken into account because the higher the moment, the harder it is to estimate. Moreover, larger sample intervals are required in order to obtain estimates of similar quality. This is due to the excess degrees of freedom consumed by the higher orders. Finally, due to the higher powers, HOS are significantly less robust than lower-order statistics.

6.6.4 Identifying NLOS samples

The detection of NLOS component in the signal depends on the statistical properties of the signal itself. As observed in the previous section, the information the algorithm wants to exploit lies in the transition between LOS and "LOS+NLOS". Therefore, the region of interest (ROI) is computed to select

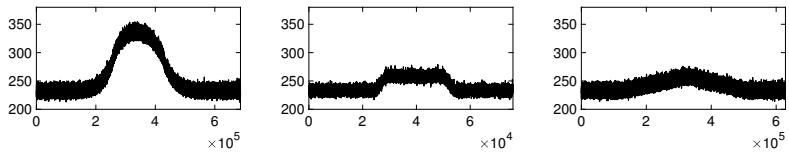

(a) Metal. (b) Glass. (c) White foamcore.

Figure 6.13: Typical signal cropped in the region of interest (ROI); sample number on x-axis and sample value on y-axis.

the subset of significant samples by searching for changes in the signal [48]. Here, a change in the signal is given by a significant variation of a statistical moment.

The ROI is selected by taking the part between the rising and falling edge and the same amount of signal before and after the statistical variation. This procedure of interval selection is performed in order to not alter the ratio between the LOS and "LOS+NLOS", and consequently, its statistical properties. Starting from the whole traces of Fig. 6.12, the signal is processed for detecting regions of interest (with a double passage back and forth, there are two ROIs) and only one ROI (since their symmetry) is selected. As examples of this procedure, the ROI for three different materials are shown in Fig. 6.13.

6.6.5 Assessment of observables to identify reflections

As a statistical analysis is performed, in Fig. 6.14 is shown the trend of each observable (μ, σ, skewness and kurtosis) over distance ("step number", where the step is constant, see Section 6.5). Since they feature different kinds of reflection, only values for glass and metal are discussed as the most interesting examples. By analyzing the results, it can be noted that μ and σ follow the same trend for both sample materials. Their values decay exponentially to the pure LOS value along distance and the only difference is in magnitude. For example the metal sample reflects more than the glass one for its particular reflective properties, bringing a strong NLOS component over all the steps. Something more peculiar can be stated for skewness and kurtosis.

In the experiment involving glass, skewness tends to zero more quickly

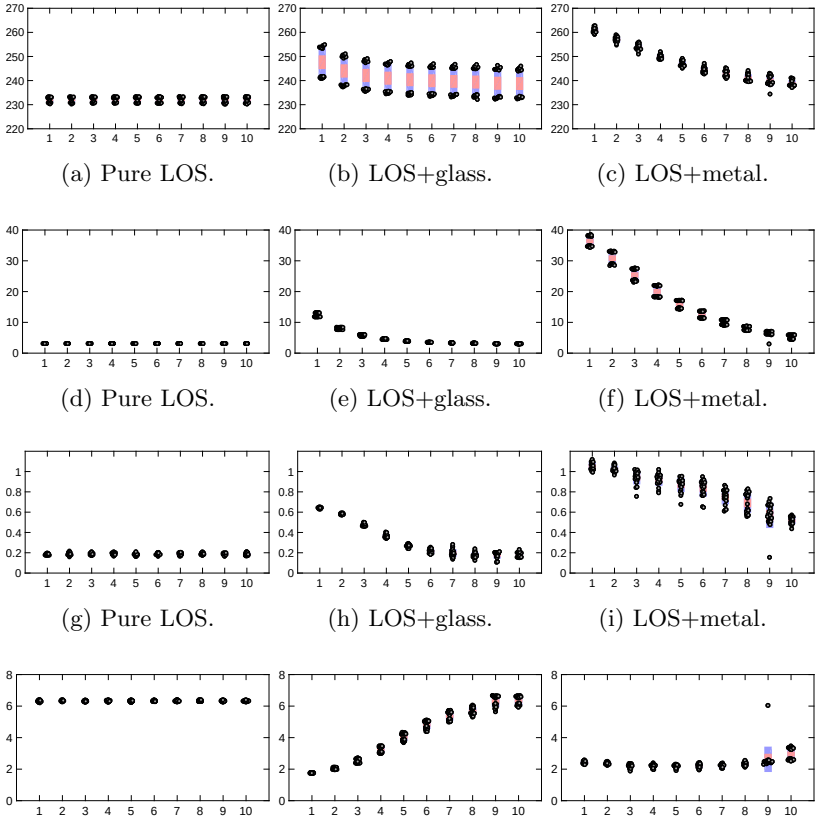

(a) Pure LOS. (b) LOS+glass. (c) LOS+metal.

(d) Pure LOS. (e) LOS+glass. (f) LOS+metal.

(g) Pure LOS. (h) LOS+glass. (i) LOS+metal.

(j) Pure LOS. (k) LOS+glass. (l) LOS+metal.

Figure 6.14: Statistical parameters μ (Fig. a-c), σ (Fig. d-f), skewness (Fig. g-i), kurtosis (Fig. j-l) and comparison among "Pure LOS" (a, d, g, j), "LOS+glass" (b, e, h, k) and "LOS+metal" (c, f, i, l). Step number on x-axis and statistical parameter value on y-axis.

Table 6.2: Example values of skew and k

Condition	skew	k
Pure LOS	0.18	6.32
LOS+metal	1.05	2.41
LOS+rwood	0.67	2.08
LOS+glass	0.64	1.77
LOS+wfoam	0.55	2.20
LOS+rwood	0.17	4.92

with respect to the one related to metal. Glass produces a reflection more directive than metal and only in a determined position along the movement. This is why the NLOS due to glass (specular-like) is lost after a few steps, becoming indistinguishable from noise. The trend for kurtosis is very different among the experiments. While in the case of metal it is quite constant just below 3, in the case of glass, it converges to 6 along distance (i.e. when the reflection contribution becomes weaker). Skewness and kurtosis values for all the scenarios acquired at "step 1" are reported in Tab. 6.2. As previously stated, "Pure LOS" condition can be identified very well by exploiting these two parameters and also an estimation of different types of reflection can be given. In particular, it can be stated that specular-like and diffuse-like reflection implies unique characteristics. The chipboard sample has very close values to the "Pure LOS" since it absorbs almost all the light and it does not produce a significant reflection, even at the closest distance. On the other hand, when a reflective material is far, the introduced NLOS component becomes weaker. This can be observed by looking at Fig. 6.15 in which, as the distance increases (marker dimension in the plot decreases), all the "LOS+NLOS" scenarios (all the markers but circles) tend to look the same, approaching the "Pure LOS" (asterisks) condition. Therefore, after a certain distance, identification cannot be performed anymore. However, in those cases, reflection due to a specific material leads to a very weak contribution and the generated noise into the system can be considered negligible.

Another important aspect to verify is the statistical analysis dependence from the object speed. The sample object is moved at the maximum speed (v1 = 1.5 km/h) and, subsequently, at half the speed (v2 = 0.75 km/h). As it can be seen from Fig. 6.16, the ROIs have the same data distribution

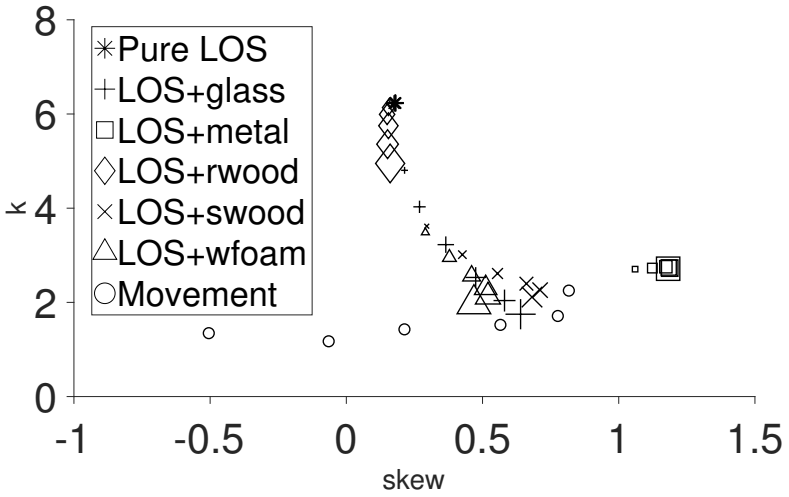

(a) Skewness vs Kurtosis.

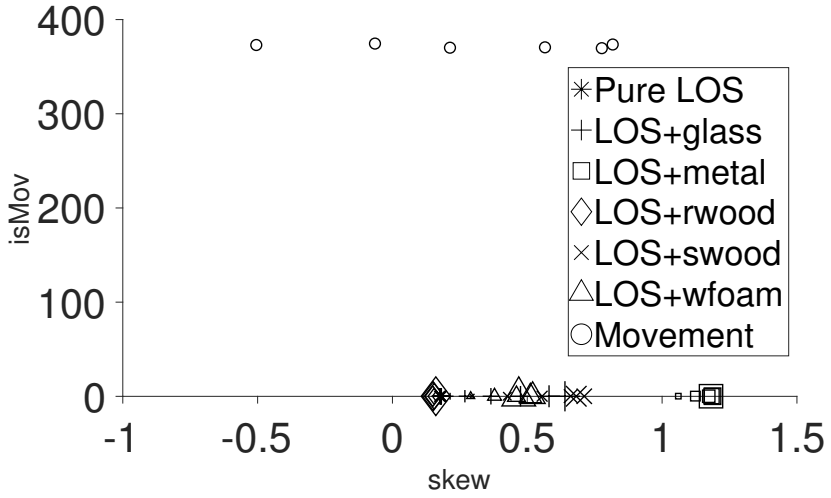

(b) Skewness vs isMov.

Figure 6.15: "Pure LOS", "LOS+NLOS" characteristics along distances and "Movement" (mean values for each step).

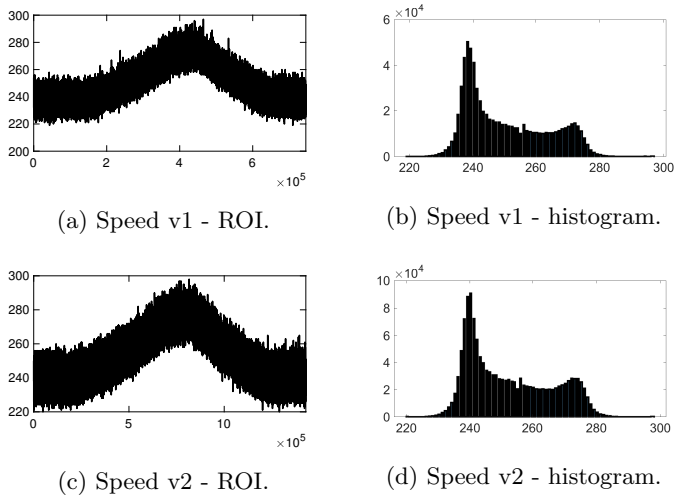

(a) Speed v1 - ROI.

(b) Speed v1 - histogram.

(c) Speed v2 - ROI.

(d) Speed v2 - histogram.

Figure 6.16: Example of object (plywood) passage at different speeds. Left to right: ROI (sample number on x-axis and sample value on y-axis), histogram (sample value on x-axis and number of occurrences on y-axis).

with same statistical values (skewness = 0.72, kurtosis = 2.11). This result fulfills the need to make the analysis speed independent. We note note that i) the absolute value of both histograms is different, because the larger the number of samples, the slower the object goes, and ii) speed independence will hold as long as the number of samples taken is large enough to contain the properties of the movement. This occurs as long as the movement is sufficiently slow compared to the sampling rate.

6.7 Multipath detection proposal

We start this section by solving the remaining problem of discerning valid RSS changes (**P1**), and then introduce a low-cost decision tree algorithm to learn which RSS sequences are caused by reflections.

6.7.1 Relative movement of devices

As seen until now, a quick object passage produces a reflection which can lead to a significant amplitude signal variation. As shown in Sec. 6.4.2 a relative linear movement between devices cannot be distinguished easily from an object. Here relative movements are investigated for understanding if a statistical analysis is still valid in detecting them. This is helpful to make sure that the presented solution does not remove information about the real position of the devices. A set of relative movements (approaching or moving away devices) at five different speeds is acquired. Figure 6.17 shows four tests performed at different speeds (v1 = 1.5 km/h and v2 = 0.38 km/h). Raw data look specular as the reflective object approaches or moves away at the same speed. Skewness assumes positive and negative values with respect to the direction of the movement, but overall both the considered statistical parameters have very similar values to those related to "LOS+NLOS" conditions, as seen in Fig. 6.14. For this reason, a way for discriminating the relative movement of devices is needed.

By considering that dynamics change fast in mobile environments and a certain NLOS component may last over a short period of time, an option would be to introduce a time metric. But this would come at the cost of a speed dependent measure, which is undesired. Here instead it is proposed to use as metric the sum of the difference between consecutive samples, called "isMov":

$$isMov = \sum_{i=2}^{N} (x_i - x_{i-1}) \tag{6.3}$$

which gives an intuition on how the system is at the end of the measuring window compared to the beginning. If they are very different, the system has changed. Else, the system relative distance did not change significantly. This let the algorithm distinguish between a signal variation which returns to the same value of the beginning after a fast perturbation (like the one coming from a reflection) and an increased final value. Typical values of "isMov" are relative high (always above 100) only for relative movements. This avoids that devices are relatively moving are not confused with a LOS to "LOS+NLOS" transition (see Fig. 6.15).

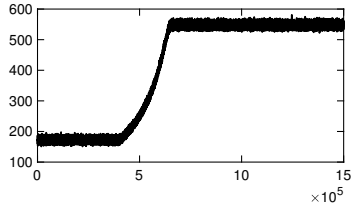

(a) Towards at speed v1 - skew = - 0.50, k = 1.34.

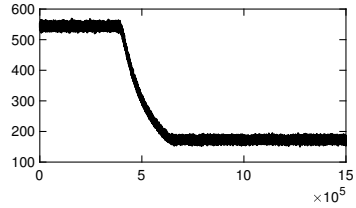

(b) Backwards at speed v1 - skew = 0.78, k = 1.72.

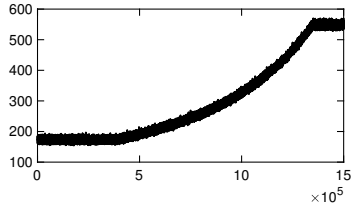

(c) Towards at speed v2 - skew = 0.82, k = 2.24.

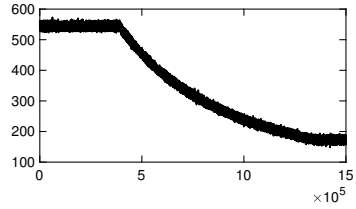

(d) Backwards at speed v2 - skew = 0.21, k = 1.43.

Figure 6.17: Typical signal for a linear movement towards and backwards the transmitter; sample number on x-axis and sample value on y-axis.

6.7.2 Insights

Skewness and kurtosis, contrary to the first and second moment, are independent of signal intensity, and they can be efficiently used as features in a classification model where three classes are discerned: "Pure LOS", "LOS+NLOS" and "Movement". Figure 6.18 shows a scatter plot of skewness vs kurtosis vs "isMov". Here, the "LOS+NLOS" class aggregates all the different materials in the tests. It can be observed that classes are well separated as the "Pure LOS" and "Movement" persist in a very limited area.

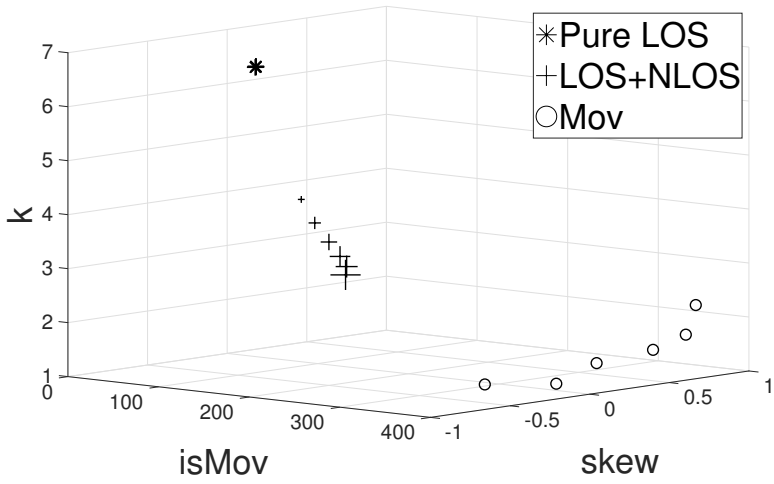

Figure 6.18: Scatter plot skewness vs kurtosis - "Pure LOS"/"LOS+NLOS".

6.7.3 Multipath detection

Here the algorithm to detect NLOS components in fully dynamic scenarios is introduced. A supervised machine learning classifier is chosen in order to classify different scenarios. The technique exploits a Decision Tree (DT) algorithm to let low-cost devices take advantage of NLOS recognition. DTs are easy to interpret, fast for fitting and prediction, and low on memory usage, but they may have low predictive accuracy. In particular, here, a coarse tree is used as it has a simple structure, fast prediction speed, small memory usage and low computational cost [62, 76]. The exploited classifica-

tion model is shown in Fig. 6.19. As mentioned before, it is a coarse tree algorithm with only two decision nodes. It uses only kurtosis and "isMov" as predictors since they are sufficient for discriminating the three labels (or classes): *"Pure LOS"*, *"LOS+NLOS"* and *"Movement"*.

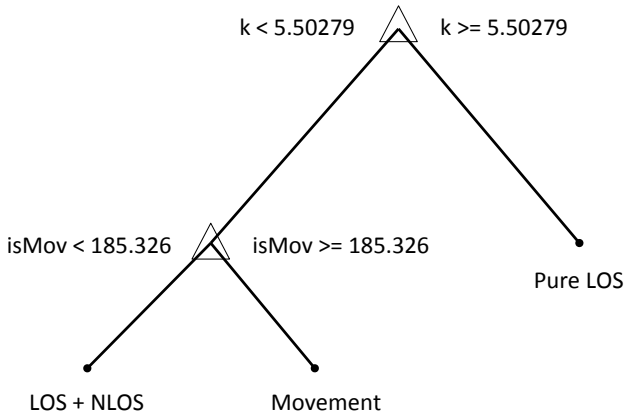

Figure 6.19: Coarse tree classification model.

For training the classification model, a data set (A) of 1320 collected observations (200 traces for each NLOS scenario and 120 for movement) is used. A 5-fold cross validation is employed for avoiding an overfitted training. The model has an accuracy of 100%. Finally, for testing the trained classification model, another different data set (B) of 660 collected observations (100 for each NLOS condition, 60 for movement) is used.

From Tab. 6.3, it can be seen how the model performs in discerning among classes. In particular, "Pure LOS" and "Movement" are always detected correctly. The "LOS+NLOS" class instead suffers the condition in which the NLOS contribution is very poor, and the classification model fails to detect it, with an error up to 26.8%. More in detail, plots of Fig. 6.20 show results when the model is tested with dataset B. Figure 6.20a reports the error along the distance of the passing object when all the steps and all the materials are considered, whereas Fig. 6.20b shows the error with all the steps included, but chipboard is not taken into account. The difference is very noticeable since in the first case, starting from the closest step, chipboard is predicted as "Pure LOS". Therefore, as expected, there are conditions with low predictive accuracy. Yet, we will show in Sec. 6.7.4 that in the scenarios where there is a higher likelihood to fail, the localization system does not suffer from the

Table 6.3: Confusion matrix, model trained on data set A and tested on data set B.

True condition		Predicted condition		
		Pure LOS	LOS+NLOS	Movement
	Pure LOS	100%	0%	0%
	LOS+NLOS	26.8%	73.2%	0%
	Movement	0%	0%	100%

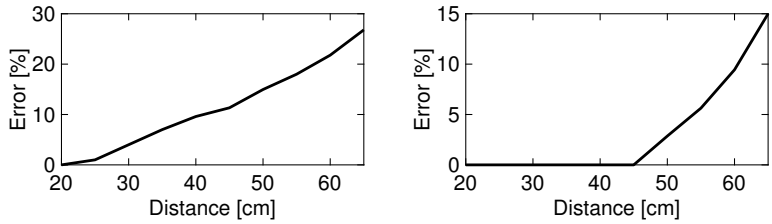

(a) Including chipboard. (b) Excluding chipboard.

Figure 6.20: Classification model error with distance.

error in the detection algorithm.

Using the results obtained in Sec. 6.7.3, a NLOS removal algorithm design is possible. This algorithm detects and corrects the NLOS components that appear in moving environments. As input, the algorithm takes the raw data from the ADC. Data are statistically analyzed and the NLOS detected using the analysis introduces in Sec. 6.7.3. Then, the NLOS component is removed, as explained in the following.

6.7.4 NLOS removal

After the statistical analysis, it is known if the signal contains a NLOS component. In order to remove it, the algorithm computes the moving average (MA) of the signal (which is given by all the components, LOS and LOS+NLOS), removes it from the signal, and it finally adds the median (M)

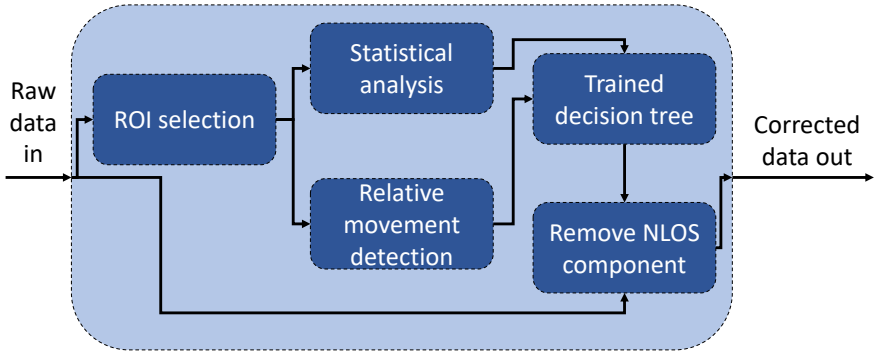

Figure 6.21: Function block of the algorithm implemented.

of the signal (only given by LOS components). That is:

$$Filtered\ signal = RAW - MA + M \tag{6.4}$$

The function block of the algorithm can be found in Fig. 6.21.

6.7.5 Algorithm Evaluation

In order to derive the performance of the NLOS removal algorithm, here, it is analysed and tested with the same data set used for localization in Fig. 6.2 of Sec. 6.4.1. As it can be seen in Fig. 6.22 and Tab.6.4, the localization error is always below 2%[7] and the accuracy increases up to 93%. The reason why the error stays low even if the relative power of the NLOS component changes is that the removal algorithm works better with higher NLOS components. In fact, when the NLOS component is low (i.e. the reflective material is far), the removal does not work very well, but the effect on the localization is, as seen in Sec. 6.4.1, negligible.

Fig.s 6.23 and 6.25 show the significant difference in terms of position accuracy among conditions and reflector distance. Overall the impact of the correction algorithm is higher when the NLOS component is stronger. In general since the system can discern, and consequently operate, among "Pure LOS", "LOS+NLOS" and movement, good results can be achieved. A prove of this is that the worst accuracy (after filtering out reflections) is 1.32 cm.

[7]Percent distance error means the positioning error w.r.t. the ground truth, that is equal and fixed to 70cm.

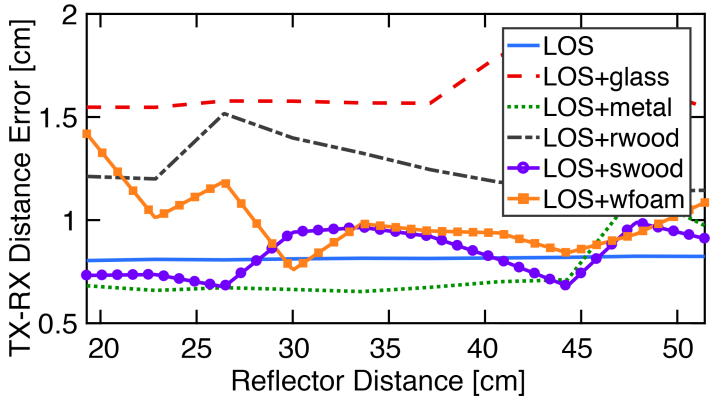

Figure 6.22: Distance calculation error after applying correction algorithm (glass = shiny glass, metal = grey satin metal, rwood = chipboard, swood = plywood, wfoam = foamcore).

Table 6.4: Position accuracy (worst cases)

Condition	W/o correction [cm]	With correction [cm]	Improvement [%]
Pure LOS	0.58	0.58	0
LOS+glass	5.15	1.32	74.3
LOS+metal	11.79	0.8	93.2
LOS+rwood	1.5	1.06	28.8
LOS+swood	4.7	0.7	85.3
LOS+wfoam	3.94	0.99	74.8

Finally the CDF (Cumulative Distribution Function) of the distance error is given in Fig.6.25a and Fig.6.25b, for positioning without and with correction respectively. By focusing on the second plot, it can be seen that with the correction algorithm the accuracy is below 1 cm almost 80% of the time.

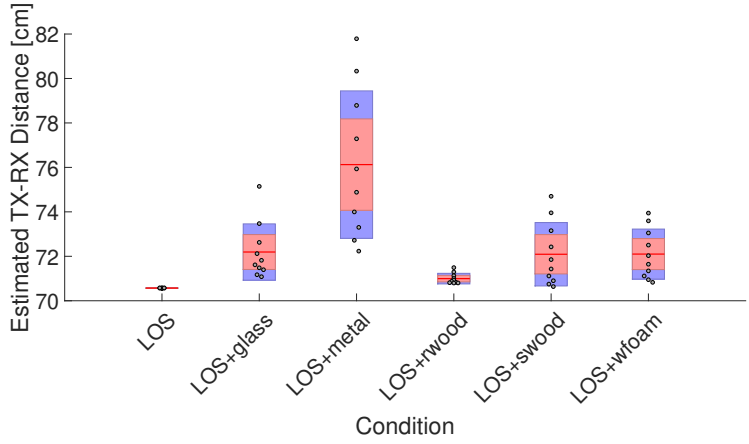

(a) Position accuracy based on different condition.

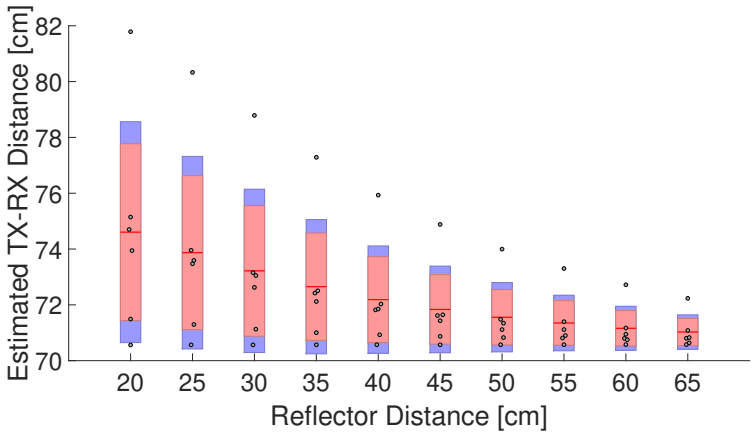

(b) Position accuracy based on different reflector distances.

Figure 6.23: LPS accuracy without correction algorithm.

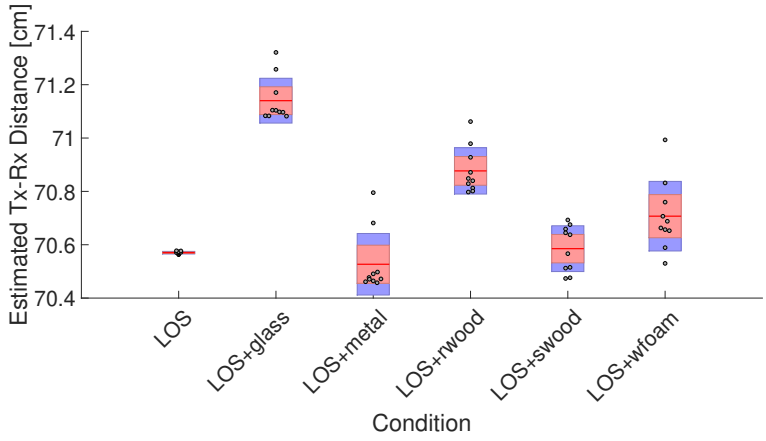

(a) Position accuracy based on different condition.

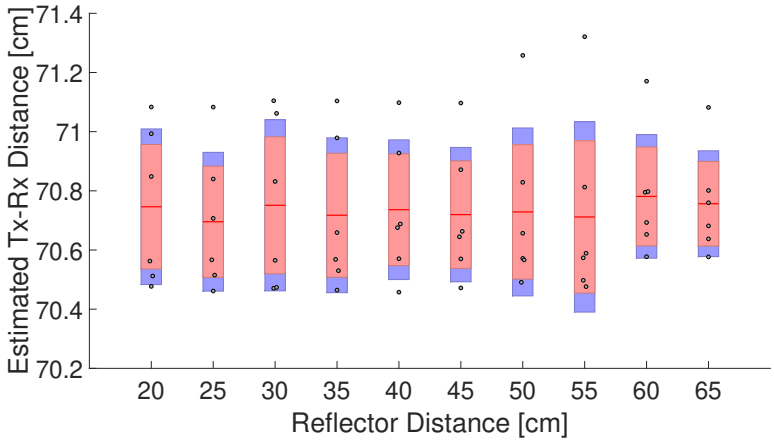

(b) Position accuracy based on different reflector distances.

Figure 6.24: LPS accuracy with correction algorithm.

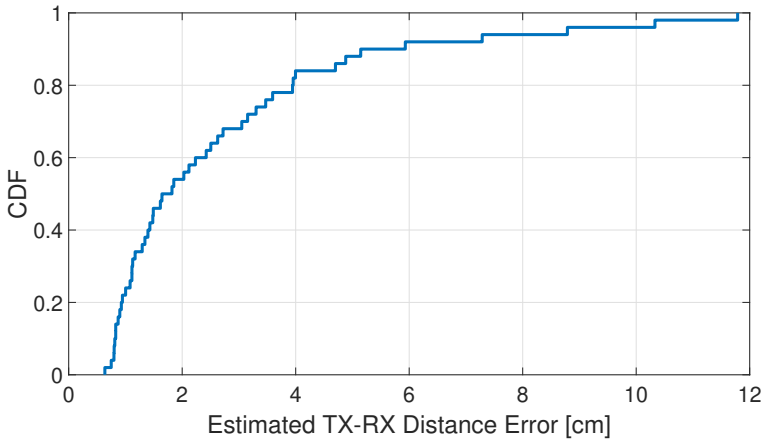

(a) Without correction algorithm.

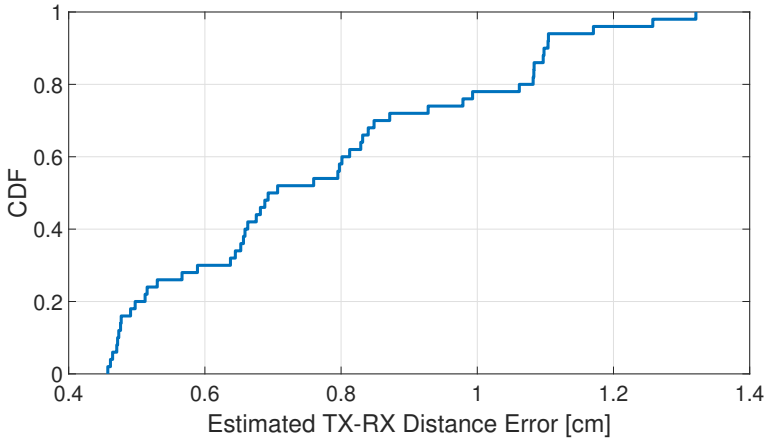

(b) With correction algorithm.

Figure 6.25: CDF of distance error.

Chapter 7

Conclusion

This chapter summarizes the contribution of the thesis and discusses avenues for future research.

7.1 Summary of contribution

The main contributions of this PhD thesis are: a preliminary study of a simple propagation VLC channel and the design and the implementation of a VLC transceiver for vehicular applications (Chapter. 5), and the introduction of a multipath detection-and-removal for LPS (Chapter. 6). The former is a preliminary work which lead to an outdoor vehicular link characterization proposal which exploits an LED-based traffic light for broadcasting messages towards vehicles. Results show that a Lambertian model that takes into account the ground reflection component fits well the experimental data and that the spatial distribution of the errors between the real measurements and the model is satisfactory. The latter presents a new multipath detection technique for positioning with light that does not require the knowledge of the channel impulse response, and that it is suited to be implemented in low-cost positioning receivers that use a single photodiode. With the introduced technique, the selected positioning algorithm accuracy increases up to 93%. This research topic has been carried out during an 11-month internship at the IMDEA Networks Institute (Leganés, Madrid, Spain).

7.2 Directions for future work

Two main guidelines are envisioned for continuing investigating the contribution introduced in this dissertation. The Infrastructure-to-Vehicle VLC link characterization with LED-based Traffic Light needs to be performed since, as mentioned in Sec. 5.1, in this thesis, only the preparatory work is presented. Basically two topics can be pursued and consist of:

1. an extensive Infrastructure-to-Vehicle experimental test campaign in realistic environments;

2. in realistic scenarios affected by multipath, processing of the acquired experimental data with the "filtering reflection" algorithm introduced in Chapter 6.

Finally, the NLOS removal technique for LPS needs to be improved and tested in different scenarios, including, for example, more reflective materials and device rotations.

Appendix A

Publications

This research activity has led to several publications in international journals and conferences. These are summarized below.[1]

International Conferences and Workshops

1. L. Mucchi and F. S. Cataliotti and L. S. Ronga and S. Caputo and **Thesis Author**. "Experimental-based propagation model for VLC", in *2017 European Conference on Networks and Communications (EuCNC)*, Oulu (Finland), 2017.

Submitted

1. **Thesis author**, A. Galisteo, M. Zuniga, L. Mucchi, D. Giustiniano. "Filtering Out Reflections in Low-cost LED-based Positioning Systems", *2019 IEEE International Conference on Computer Communications (INFOCOM)*, 2018.

National Conferences

1. **Thesis Author**. "Channel Modeling for Vehicular Visible Light Communications", in *GTTI, Poster Session*, Udine, Italy, 2017.

[1]The author's bibliometric indices are the following: H-index = 3, total number of citations = 52 (source: Google Scholar on Month 10, 2018).

Bibliography

[1] "Ieee standard for local and metropolitan area networks–part 15.7: Short-range wireless optical communication using visible light," *IEEE Std 802.15.7-2011*, pp. 1–309, Sept 2011.

[2] "Ieee guide for wireless access in vehicular environments (wave) - architecture," *IEEE Std 1609.0-2013*, pp. 1–78, March 2014.

[3] (2018) Acro system. Available at https://openbuilds.com/builds/openbuilds-acro-system.5416/.

[4] (2018) Beaglebone black. Available at https://beagleboard.org/black.

[5] (2018) Gnu radio. Available at https://www.gnuradio.org.

[6] (2018) Ledinside: Top 10 led demand and supply market trends in 2018. [Online]. Available: http://www.ledinside.com

[7] (2018) Openvlc. Available at http://www.openvlc.org.

[8] (2018) Philips indoor positioning. [Online]. Available: http://www.lighting.philips.com/main/systems/lighting-systems/indoor-positioning

[9] (2018) Usrp1. Available at https://www.ettus.com/product/details/USRPPKG.

[10] (2018) Zemax. Available at http://www.zemax.com.

[11] M. Akanegawa, Y. Tanaka, and M. Nakagawa, "Basic study on traffic information system using led traffic lights," *IEEE Transactions on Intelligent Transportation Systems*, vol. 2, no. 4, pp. 197–203, Dec 2001.

[12] M. T. Alresheedi, A. T. Hussein, and J. M. H. Elmirghani, "Uplink design in vlc systems with ir sources and beam steering," *IET Communications*, vol. 11, no. 3, pp. 311–317, 2017.

[13] N. Araki and H. Yashima, "A channel model of optical wireless communications during rainfall," in *2005 2nd International Symposium on Wireless Communication Systems*, Sept 2005, pp. 205–209.

[14] M. Ayyash, H. Elgala, A. Khreishah, V. Jungnickel, T. Little, S. Shao, M. Rahaim, D. Schulz, J. Hilt, and R. Freund, "Coexistence of wifi and lifi toward 5g: concepts, opportunities, and challenges," *IEEE Communications Magazine*, vol. 54, no. 2, pp. 64–71, February 2016.

[15] J. R. Barry, J. M. Kahn, W. J. Krause, E. A. Lee, and D. G. Messerschmitt, "Simulation of multipath impulse response for indoor wireless optical channels," *IEEE Journal on Selected Areas in Communications*, vol. 11, no. 3, pp. 367–379, Apr 1993.

[16] D. A. Basnayaka and H. Haas, "Hybrid rf and vlc systems: Improving user data rate performance of vlc systems," in *2015 IEEE 81st Vehicular Technology Conference (VTC Spring)*, May 2015, pp. 1–5.

[17] S. Brown, *Measures of Shape: Skewness and Kurtosis*. Oak Road Systems, 2018. [Online]. Available: https://brownmath.com/stat/shape.htm

[18] T. C. Bui and S. Kiravittaya, "Demonstration of using camera communication based infrared led for uplink in indoor visible light communication," in *2016 IEEE Sixth International Conference on Communications and Electronics (ICCE)*, July 2016, pp. 71–76.

[19] A. Cailean, B. Cagneau, L. Chassagne, M. Dimian, and V. Popa, "Novel receiver sensor for visible light communications in automotive applications," *IEEE Sensors Journal*, vol. 15, no. 8, pp. 4632–4639, Aug 2015.

[20] A. Cailean, B. Cagneau, L. Chassagne, S. Topsu, Y. Alayli, and J. M. Blosseville, "Visible light communications: Application to cooperation between vehicles and road infrastructures," in *2012 IEEE Intelligent Vehicles Symposium*, June 2012, pp. 1055–1059.

[21] A. Cailean and M. Dimian, "Toward environmental-adaptive visible light communications receivers for automotive applications: A review," *IEEE Sensors Journal*, vol. 16, no. 9, pp. 2803–2811, May 2016.

[22] ——, "Impact of ieee 802.15.7 standard on visible light communications usage in automotive applications," *IEEE Communications Magazine*, pp. 2–7, 2018.

[23] A. L. Chen, H. P. Wu, Y. L. Wei, and H. M. Tsai, "Time variation in vehicle-to-vehicle visible light communication channels," in *2016 IEEE Vehicular Networking Conference (VNC)*, Dec 2016, pp. 1–8.

[24] C. Chen, D. Basnayaka, and H. Haas, "Non-line-of-sight channel impulse response characterisation in visible light communications," in *2016 IEEE International Conference on Communications (ICC)*, May 2016, pp. 1–6.

[25] C. Chen, D. A. Basnayaka, X. Wu, and H. Haas, "Efficient analytical calculation of non-line-of-sight channel impulse response in visible light communications," *Journal of Lightwave Technology*, vol. 36, no. 9, pp. 1666–1682, May 2018.

[26] J. Chen and C. Yan, "A channel model for indoor visible light communication system with specular reflection," in *2017 16th International Conference on Optical Communications and Networks (ICOCN)*, Aug 2017, pp. 1–3.

[27] H. Chun, S. Rajbhandari, G. Faulkner, D. Tsonev, H. Haas, and D. O'Brien, "Demonstration of a bi-directional visible light communication with an overall sum-rate of 110 mb/s using leds as emitter and detector," in *2014 IEEE Photonics Conference*, Oct 2014, pp. 132–133.

[28] K. Cui, G. Chen, Z. Xu, and R. D. Roberts, "Experimental characterization of traffic light to vehicle vlc link performance," in *2011 IEEE GLOBECOM Workshops (GC Wkshps)*, Dec 2011, pp. 808–812.

[29] Z. Cui, C. Wang, and H. M. Tsai, "Characterizing channel fading in vehicular visible light communications with video data," in *2014 IEEE Vehicular Networking Conference (VNC)*, Dec 2014, pp. 226–229.

[30] Z. Cui, S. W. Yang, and H. M. Tsai, "A vision-based hierarchical framework for autonomous front-vehicle taillights detection and signal recognition," in *2015 IEEE 18th International Conference on Intelligent Transportation Systems*, Sept 2015, pp. 931–937.

[31] P. Dietz, W. Yerazunis, and D. Leigh, "Very low-cost sensing and communication using bidirectional leds," in *UbiComp 2003: Ubiquitous Computing*. Berlin, Heidelberg: Springer Berlin Heidelberg, 2003, pp. 175–191.

[32] D.-q. Ding and X.-z. Ke, "A new indoor vlc channel model based on reflection," *Optoelectronics Letters*, vol. 6, no. 4, pp. 295–298, Jul 2010. [Online]. Available: https://doi.org/10.1007/s11801-010-0028-1

[33] Z. Dong, T. Shang, Y. Gao, and Q. Li, "Study on vlc channel modeling under random shadowing," *IEEE Photonics Journal*, vol. 9, no. 6, pp. 1–16, Dec 2017.

[34] L. Feng, R. Q. Hu, J. Wang, P. Xu, and Y. Qian, "Applying vlc in 5g networks: Architectures and key technologies," *IEEE Network*, vol. 30, no. 6, pp. 77–83, November 2016.

[35] M. Fox, *Optical properties of solids (2nd ed.)*. Oxford: Oxford University Press, 2010.

[36] A. Galisteo, Q. Wang, A. Deshpande, M. Zuniga, and D. Giustiniano, "Follow that light: Leveraging leds for relative two-dimensional localization," in *Proceedings of the 13th International Conference on Emerging Networking EXperiments and Technologies*, ser. CoNEXT '17. New York, NY, USA: ACM, 2017, pp. 187–198. [Online]. Available: http://doi.acm.org/10.1145/3143361.3143371

[37] S. Gong, M. Zhang, and Y. Zhang, "Research on influence of diffuse reflection on indoor visible light communication transmission rate," in *2014 OptoElectronics and Communication Conference and Australian Conference on Optical Fibre Technology*, July 2014, pp. 447–449.

[38] W. Gu, M. Aminikashani, P. Deng, and M. Kavehrad, "Impact of multipath reflections on the performance of indoor visible light positioning systems," *Journal of Lightwave Technology*, vol. 34, no. 10, pp. 2578–2587, May 2016.

[39] W. Gu, M. Aminikashani, and M. Kavehrad, "Indoor visible light positioning system with multipath reflection analysis," in *2016 IEEE International Conference on Consumer Electronics (ICCE)*, Jan 2016, pp. 89–92.

[40] N. U. Hassan, A. Naeem, M. A. Pasha, T. Jadoon, and C. Yuen, "Indoor positioning using visible led lights: A survey," *ACM Comput. Surv.*, vol. 48, no. 2, pp. 20:1–20:32, Nov. 2015. [Online]. Available: http://doi.acm.org/10.1145/2835376

[41] H. Hosseinianfar, M. Noshad, and M. Brandt-Pearce, "Positioning for visible light communication system exploiting multipath reflections," in *2017 IEEE International Conference on Communications (ICC)*, May 2017, pp. 1–6.

[42] P. Hu *et al.*, "Colorbars: Increasing data rate of led-to-camera communication using color shift keying," in *ACM CoNEXT*, 2015.

[43] C. Huang and X. Zhang, "Los-nlos identification algorithm for indoor visible light positioning system," in *2017 20th International Symposium on Wireless Personal Multimedia Communications (WPMC)*, Dec 2017, pp. 575–578.

[44] S. Iwasaki, C. Premachandra, T. Endo, T. Fujii, M. Tanimoto, and Y. Kimura, "Visible light road-to-vehicle communication using high-speed camera," in *2008 IEEE Intelligent Vehicles Symposium*, June 2008, pp. 13–18.

[45] S. Jung, S. Hann, and C. Park, "Tdoa-based optical wireless indoor localization using led ceiling lamps," *IEEE Transactions on Consumer Electronics*, vol. 57, no. 4, pp. 1592–1597, November 2011.

[46] D. Karunatilaka, F. Zafar, V. Kalavally, and R. Parthiban, "Led based indoor visible light communications: State of the art," *IEEE Communications Surveys Tutorials*, vol. 17, no. 3, pp. 1649–1678, thirdquarter 2015.

[47] M. F. Keskin, A. D. Sezer, and S. Gezici, "Localization via visible light systems," *Proceedings of the IEEE*, vol. 106, no. 6, pp. 1063–1088, June 2018.

[48] R. Killick *et al.*, "Optimal detection of changepoints with a linear computational cost," *ArXiv e-prints*, 2011.

[49] Y. H. Kim, W. A. Cahyadi, and Y. H. Chung, "Experimental demonstration of vlc-based vehicle-to-vehicle communications under fog conditions," *IEEE Photonics Journal*, vol. 7, no. 6, pp. 1–9, Dec 2015.

[50] M. Kinoshita, T. Yamazato, H. Okada, T. Fujii, S. Arai, T. Yendo, and K. Kamakura, "Channel fluctuation measurement for image sensor based i2v-vlc, v2i-vlc, and v2v-vlc," in *2014 IEEE Asia Pacific Conference on Circuits and Systems (APCCAS)*, Nov 2014, pp. 332–335.

[51] N. Kumar, "Visible light communication based traffic information broadcasting systems," *International Journal of Future Computer and Communication*, vol. 2, no. 6, pp. 26–30, 2014.

[52] Y.-S. Kuo *et al.*, "Luxapose: Indoor positioning with mobile phones and visible light," in *ACM MobiCom*, 2014.

[53] I. E. Lee, M. L. Sim, and F. W. L. Kung, "Performance enhancement of outdoor visible-light communication system using selective combining receiver," *IET Optoelectronics*, vol. 3, no. 1, pp. 30–39, February 2009.

[54] S. J. Lee, J. K. Kwon, S. Y. Jung, and Y. H. Kwon, "Simulation modeling of visible light communication channel for automotive applications," in *2012 15th International IEEE Conference on Intelligent Transportation Systems*, Sept 2012, pp. 463–468.

[55] L. Li, P. Hu, C. Peng, G. Shen, and F. Zhao, "Epsilon: A visible light based positioning system," in *11th USENIX Symposium on Networked Systems Design and Implementation (NSDI 14)*. Seattle, WA: USENIX Association, 2014, pp. 331–343. [Online]. Available: https://www.usenix.org/conference/nsdi14/technical-sessions/presentation/li

[56] R. LiKamWa *et al.*, "Energy characterization and optimization of image sensing toward continuous mobile vision," in *ACM MobiSys*, 2013.

[57] C. B. Liu, B. Sadeghi, and E. W. Knightly, "Enabling vehicular visible light communication (v2lc) networks," in *Proceedings of the Eighth ACM International Workshop on Vehicular Inter-networking*, ser. VANET '11. New York, NY, USA: ACM, 2011, pp. 41–50. [Online]. Available: http://doi.acm.org/10.1145/2030698.2030705

[58] C. R. Lomba, R. T. Valadas, and A. M. d. O. Duarte, "Experimental characterisation and modelling of the reflection of infrared signals on indoor surfaces," *IEE Proceedings - Optoelectronics*, vol. 145, no. 3, pp. 191–197, Jun 1998.

[59] J. Luo, L. Fan, and H. Li, "Indoor positioning systems based on visible light communication: State of the art," *IEEE Communications Surveys Tutorials*, vol. 19, no. 4, pp. 2871–2893, Fourthquarter 2017.

[60] P. Luo, Z. Ghassemlooy, H. L. Minh, E. Bentley, A. Burton, and X. Tang, "Fundamental analysis of a car to car visible light communication system," in *2014 9th International Symposium on Communication Systems, Networks Digital Sign (CSNDSP)*, July 2014, pp. 1011–1016.

[61] M. H. A. M. A. Elkarim, N. A. Mohammed, "Exploring the performance of indoor localization systems based on vlc-rssi, including the effect of nlos components using two light-emitting diode lighting systems," *Optical Engineering*, vol. 54, no. 10, pp. 105 110–1 – 105 110–9, 2015. [Online]. Available: https://doi.org/10.1117/1.OE.54.10.105110

[62] A. Mannini *et al.*, "Machine learning methods for classifying human physical activity from on-body accelerometers," *Sensors*, 2010.

[63] A. Memedi, H. M. Tsai, and F. Dressler, "Impact of realistic light radiation pattern on vehicular visible light communication," in *GLOBECOM 2017 - 2017 IEEE Global Communications Conference*, Dec 2017, pp. 1–6.

[64] F. Miramirkhani, O. Narmanlioglu, M. Uysal, and E. Panayirci, "A mobile channel model for vlc and application to adaptive system design," *IEEE Communications Letters*, vol. 21, no. 5, pp. 1035–1038, May 2017.

[65] N. A. Mohammed and M. A. Elkarim, "Exploring the effect of diffuse reflection on indoor localization systems based on rssi-vlc," *Opt. Express*, vol. 23, no. 16, pp. 20 297–20 313, Aug 2015. [Online]. Available: http://www.opticsexpress.org/abstract.cfm?URI=oe-23-16-20297

[66] Y. L. Morgan, "Notes on dsrc amp;amp; wave standards suite: Its architecture, design, and characteristics," *IEEE Communications Surveys Tutorials*, vol. 12, no. 4, pp. 504–518, Fourth 2010.

[67] L. Mucchi, F. S. Cataliotti, L. Ronga, S. Caputo, and P. Marcocci, "Experimental-based propagation model for vlc," in *2017 European Conference on Networks and Communications (EuCNC)*, June 2017, pp. 1–5.

[68] U. Nadeem, N. U. Hassan, M. A. Pasha, and C. Yuen, "Highly accurate 3d wireless indoor positioning system using white led lights," *Electronics Letters*, vol. 50, no. 11, pp. 828–830, May 2014.

[69] S. Naribole, S. Chen, E. Heng, and E. Knightly, "Lira: A wlan architecture for visible light communication with a wi-fi uplink," in *2017 14th Annual IEEE International Conference on Sensing, Communication, and Networking (SECON)*, June 2017, pp. 1–9.

[70] S. Okada, T. Yendo, T. Yamazato, T. Fujii, M. Tanimoto, and Y. Kimura, "On-vehicle receiver for distant visible light road-to-vehicle communication," in *2009 IEEE Intelligent Vehicles Symposium*, June 2009, pp. 1033–1038.

[71] W. H. Org., Ed., *Global status report on road safety 2015.* WHO, 2015.

[72] W. Pan, Y. Hou, and S. Xiao, "Visible light indoor positioning based on camera with specular reflection cancellation," in *2017 Conference on Lasers and Electro-Optics Pacific Rim (CLEO-PR)*, July 2017, pp. 1–4.

[73] P. H. Pathak, X. Feng, P. Hu, and P. Mohapatra, "Visible light communication, networking, and sensing: A survey, potential and challenges," *IEEE Communications Surveys Tutorials*, vol. 17, no. 4, pp. 2047–2077, Fourthquarter 2015.

[74] B. T. Phong, "Illumination for computer generated pictures," *Communications of the ACM*, 1975.

[75] C. Sommer. (2017) Veins. Available at http://veins.car2x.org.

[76] M. Susi *et al.*, "Accelerometer signal features and classification algorithms for positioning applications," *Proceedings of the 2011 International Technical Meeting of The Institute of Navigation*, 2011.

[77] W. Tang, J. Zhang, B. Chen, Y. Liu, Y. Zuo, S. Liu, and Y. Dai, "Analysis of indoor vlc positioning system with multiple reflections," in *2017 16th International Conference on Optical Communications and Networks (ICOCN)*, Aug 2017, pp. 1–3.

[78] H.-Y. Tseng, Y. L. Wei, A.-L. Chen, H.-P. Wu, H. Hsu, and H. M. Tsai, "Characterizing link asymmetry in vehicle-to-vehicle visible light communications," in *2015 IEEE Vehicular Networking Conference (VNC)*, Dec 2015, pp. 88–95.

[79] B. Turan, S. Ucar, S. C. Ergen, and O. Ozkasap, "Dual channel visible light communications for enhanced vehicular connectivity," in *2015 IEEE Vehicular Networking Conference (VNC)*, Dec 2015, pp. 84–87.

[80] M. Uysal, Z. Ghassemlooy, A. Bekkali, A. Kadri, and H. Menouar, "Visible light communication for vehicular networking: Performance study of a v2v system using a measured headlamp beam pattern model," *IEEE Vehicular Technology Magazine*, vol. 10, no. 4, pp. 45–53, Dec 2015.

[81] W. Viriyasitavat, S. Yu, and H. Tsai, "Short paper: Channel model for visible light communications using off-the-shelf scooter taillight," in *2013 IEEE Vehicular Networking Conference*, Dec 2013, pp. 170–173.

[82] Q. Wang, D. Giustiniano, and D. Puccinelli, "An open source research platform for embedded visible light networking," *IEEE Wireless Communications*, vol. 22, no. 2, pp. 94–100, April 2015.

[83] H. B. C. Wook, T. Komine, S. Haruyama, and M. Nakagawa, "Visible light communication with led-based traffic lights using 2-dimensional image sensor," in *CCNC 2006. 2006 3rd IEEE Consumer Communications and Networking Conference, 2006.*, vol. 1, Jan 2006, pp. 243–247.

[84] L. C. Wu and H. M. Tsai, "Modeling vehicle-to-vehicle visible light communication link duration with empirical data," in *2013 IEEE Globecom Workshops (GC Wkshps)*, Dec 2013, pp. 1103–1109.

[85] J. Xu, H. Shen, W. Xu, H. Zhang, and X. You, "Led-assisted three-dimensional indoor positioning for multiphotodiode device interfered by multipath reflections," in *2017 IEEE 85th Vehicular Technology Conference (VTC Spring)*, June 2017, pp. 1–6.

[86] Q. Yang, C. Hsiao-Hwa, and M. Wei-Xiao, "Channel modeling for visible light communications - a survey," *Wireless Communications and Mobile Computing*, vol. 16, no. 14, pp. 2016–2034, 2016. [Online]. Available: https://onlinelibrary.wiley.com/doi/abs/10.1002/wcm.2665

[87] M. Yasir *et al.*, "Indoor positioning system using visible light and accelerometer," *IEEE Journal of Lightwave Technology*, 2014.

[88] J.-H. Yoo, R. Lee, J.-K. Oh, H.-W. Seo, J.-Y. Kim, H.-C. Kim, and S.-Y. Jung, "Demonstration of vehicular visible light communication based on led headlamp," in *2013 Fifth International Conference on Ubiquitous and Future Networks (ICUFN)*, July 2013, pp. 465–467.

[89] Y. Zhuang, L. Hua, L. Qi, J. Yang, P. Cao, Y. Cao, Y. Wu, J. Thompson, and H. Haas, "A survey of positioning systems using visible led lights," *IEEE Communications Surveys Tutorials*, pp. 1–1, 2018.